Don Pedro Relicensing

W&AR-03 and W&AR-16
River/Reservoir Temperature Models Meetings

Consultation Meetings Log

Meeting Description	No.	Meeting Date
Reservoir Temperature Model	1	04/10/2012
River/Reservoir Temperature Models	2	10/26/2012
River/Reservoir Temperature Models	3	06/04/2013

April 10, 2012 Reservoir Temperature Model Meeting No. 1 Documents:

DATE	FROM	TO	SUBJECT
02/07/2012	Rose Staples, HDR	Relicensing Participants	Proposed Workshops/Meetings Schedule for 2012
04/02/2012	Rose Staples, HDR	Relicensing Participants	Agenda and Advance Materials
04/06/2012	Rose Staples, HDR	Relicensing Participants	Logistics
07/26/2012	Rose Staples, HDR	Relicensing Participants	Draft Meeting Notes for 30-Day Review and Comment; no comments received; Draft Meeting Notes are considered final and are being filed with FERC here as part this Draft License Application

October 26, 2012 (postponed from September 18, 2012) River/Reservoir Temperature Models Meeting No. 2 documents:

DATE	FROM	TO	SUBJECT
07/26/2012	Rose Staples, HDR	Relicensing Participants	Announcement of New Date
10/18/2012	Rose Staples, HDR	Relicensing Participants	Agenda and Advance Materials
10/23/2012	Rose Staples, HDR	Relicensing Participants	Additional Advance Materials
10/24/2012	Rose Staples, HDR	Relicensing Participants	Logistics
10/26/2012	Rose Staples, HDR	Relicensing Participants	Update of Meeting Agenda Timing—running ahead of schedule
12/14/2012	Rose Staples, HDR	Relicensing Participants	Draft Meeting Notes for 30-Day Review and Comment

DATE	FROM	TO	SUBJECT
04/09/2013	Districts	FERC	Final Meeting Notes filed with FERC as part of the Districts' Response to Relicensing Participants Comments on the Initial Study Report

June 4, 2013 River/Reservoir Temperature Models Meeting No. 3 Documents:

DATE	FROM	TO	SUBJECT
05/29/2013	Rose Staples, HDR	Relicensing Participants	Advance Materials
06/26/2013	Rose Staples, HDR	Relicensing Participants	Draft Meeting Notes for 30-Day Review and Comment
07/19/2013	Jeffrey Single, CDFW	Districts	Comments on Draft Meeting Notes, as well as comments on W&AR-02 May 30, 2013 Workshop
10/04/2013	Districts	FERC	Districts' Response to CDFW Comments

W&AR-03

Temperature Model Meeting No. 1

April 10, 2012

From: Staples, Rose

Sent: Tuesday, February 07, 2012 8:15 PM

To: Alves, Jim - City of Modesto; Anderson, Craig - USFWS; Asay, Lynette - N-R; Aud, John - SCERD; Barnes, James - BLM; Barnes, Peter - SWRCB; Beuttler, John - CSPA; Blake, Martin; Bond, Jack - City of Modesto; Boucher, Allison - TRC; Boucher, Dave - Allison - TRC; Bowes, Stephen - NPS; Bowman, Art - CWRMP; Brenneman, Beth - BLM; Brewer, Doug - TetraTech; Brochini, Anthony - SSMN; Brochini, Tony - NPS; Buckley, John - CSERC; Buckley, Mark; Burley, Silvia-CVMT; Burt, Charles - CalPoly; Cadagan, Jerry; Carlin, Michael - SFPUC; Catlett, Kelly - FOR; Charles, Cindy - GWWF; Cismowski, Gail - SWRCB; Costa, Jan - Chicken Ranch; Cowan, Jeffrey; Cox, Stanley Rob - TBMWI; Cranston, Peggy - BLM; Cremeen, Rebecca - CSERC; Day, Kevin - TBMI; Day, P - MF; Denean - BVR; Derwin, Maryann Moise; Devine, John; Donaldson, Milford Wayne - OHP; Dowd, Maggie-SNF; Drekmeier, Peter - TRT; Edmondson, Steve - NOAA; Eicher, James - BLM; Fety, Lauren - BLM; Findley, Timothy - Hanson Bridgett; Freeman, Beau - CalPoly; Fuller, Reba - TMTC; Furman, Donn W - SFPUC; Ganteinbein, Julie - Water-Power Law Grp; Giglio, Deborah - USFWS; Gorman, Elaine - YSC; Grader, Zeke; Gutierrez, Monica - NOAA-NMFS; Hackamack, Robert; Hastreiter, James L - FERC; Hatch, Jenny - CT; Hayat, Zahra - MF; Hayden, Ann; Hellam, Anita - HH; Heyne, Tim - CDFG; Holden, James ; Holm, Lisa; Horn, Jeff - BLM; Horn, Tini; Hudelson, Bill - StanislausFoodProducts; Hughes, Noah; Hughes, Robert - CDFG; Hume, Noah - Stillwater; Jackman, Jerry ; Jackson, Zac - USFWS; Jennings, William - CSPA; Jensen, Art - BAWSCA; Jensen, Laura - TNC; Johannis, Mary; Johnson, Brian - CalTrout; Justin; Keating, Janice; Kempton, Kathryn - NOAA-MNFS; Kinney, Teresa; Koepele, Patrick - TRT; Kordella, Lesley - FERC; Lein, Joseph; Levin, Ellen - SFPUC; Lewis-Reggie-PRCI; Linkard, David - TRT /RH; Looker, Mark - LCC; Loy, Carin; Lwenya, Roselynn, BVR; Lyons, Bill - MR; Madden, Dan; Manji, Annie; Marko, Paul ; Marshall, Mike - RHH; Martin, Michael - MFFC; Martin, Ramon - USFWS; Mathiesen, Lloyd - CRRMW; McDaniel, Dan -CDWA; McDevitt, Ray - BAWSCA; McDonnell, Marty - SMRT; McLain, Jeffrey - NOAA-NMFS; Means, Julie - CDFG; Mills, John - TUD; Morningstar Pope, Rhonda - BVR; Motola, Mary - PRCI; O'Brien, Jennifer - CDFG; Orvis, Tom - SCFB; Ott, Bob; Ott, Chris; Paul, Duane - Cardno; Pavich, Steve-Cardno; Pinhey, Nick - City of Modesto; Pool, Richard; Porter, Ruth - RHH; Powell, Melissa - CRRMW; Puccini, Stephen - CDFG; Raeder, Jessie - TRT; Ramirez, Tim - SFPUC; Rea, Maria - NOAA-NMFS; Reed, Rhonda - NOAA-NMFS; Richardson, Kevin - USACE; Ridenour, Jim; Robbins, Royal; Romano, David O - N-R; Roos-Collins, Richard - Water-Power Law Grp for NHI; Roseman, Jesse; Rothert, Steve - AR; Sander, Max - TNC; Sandkulla, Nicole - BAWSCA; Saunders, Jenan; Schutte, Allison - HB; Sears, William - SFPUC; Shakal, Sarah - Humboldt State; Shipley, Robert; Shumway, Vern - SNF; Shutes, Chris - CSPA; Sill, Todd; Slay, Ronn - CNRF/AIC; Smith, Jim - MPM; Staples, Rose; Steindorf, Dave - AW; Steiner, Dan; Stone, Vicki -TBMI; Stork, Ron - FOR; Stratton, Susan - CA SHPO; Taylor, Mary Jane - CDFG; Terpstra, Thomas; TeVelde, George A ; Thompson, Larry - NOAA-MNFS; Vasquez, Sandy ; Verkuil, Colette - TRT/MF; Vierra, Chris; Villalabos, Ruben; Walters, Eric - MF; Wantuck, Rick - NOAA-NMFS; Welch, Steve - ARTA; Wesselman, Eric - TRT; Wheeler, Dan; Wheeler, Dave; Wheeler, Douglas - RHH; Wilcox, Scott - Stillwater; Williamson, Harry (NPS); Willy, Alison - FWS; Wilson, Bryan - MF; Winchell, Frank - FERC; Wood, Dave - FR; Wooster, John -NOAA; Workman, Michelle - USFWS; Yoshiyama, Ron; Zipser, Wayne - SCFB

Subject: Don Pedro Project Relicensing Water & Aquatic Study Plans Workshop/Meeting Schedule for 2012

In accordance with FERC's Study Plan Determination and the Districts' Water & Aquatic (W&AR) study plans to be underway in 2012, we have developed schedule dates for the various workshops contained within the study plans. Please make note of these below:

April 2012

Apr 09 1:00 pm - 5:00 pm PT Don Pedro Project Relicensing - Hydrology Workshop (W&AR-2) (Modesto Irrigation District Offices, Modesto {MID})

Apr 10 8:00 am – 10:00 am PT Don Pedro Project Relicensing - Reservoir Temperature Modeling Data and Methods (MID)

Apr 10 10:15 am - 5:00 pm PT Don Pedro Project Relicensing - Salmonid Population Information Workshop (W&AR-5) (MID)

June 2012

Jun 26 9:00 am – 4:00 pm PT Don Pedro Project Relicensing - Salmonid Population Information Workshop (W&AR-5) (MID)

September 2012

Sep 18 9:00 am - 4:00 pm PT Don Pedro Project Relicensing - Temperature Model Verification/Calibration Meeting (MID)

November 2012

Nov 15 9:00 am - 4:00 pm PT Don Pedro Project Relicensing - Chinook Population (W&AR-6) and O.mykiss Population

(W&AR-10) Modeling Workshop (MID)

In addition, in accordance with FERC's direction regarding the development and implementation of a more explicit consultation program for those studies with workshops, we are proposing to hold a meeting on March 20th at MID (from 1:30 to 4:30 p.m.) to discuss and finalize such a Workshop Consultation Program. An initial proposal will be forwarded by March 5 to all participants.

March 2012

Mar 20 1:30 pm – 4:30 pm PT Don Pedro Project Relicensing - Workshop on Consultation Process (as per Appendix B of FERC's Study Plan Determination) (MID)

We look forward to continuing to work with all relicensing participants in 2012.

ROSE STAPLES
CAP-OM

HDR Engineering, Inc.
Executive Assistant, Hydropower Services

970 Baxter Boulevard, Suite 301 | Portland, ME 04103
207.239.3857 | f: 207.775.1742
rose.staples@hdrinc.com | hdrinc.com

From: Staples, Rose
Sent: Monday, April 02, 2012 7:41 PM
To: 'Alves, Jim'; 'Anderson, Craig'; 'Asay, Lynette'; 'Aud, John'; 'Barnes, James'; 'Barnes, Peter'; 'Blake, Martin'; 'Bond, Jack'; Borovansky, Jenna; 'Boucher, Allison'; 'Bowes, Stephen'; 'Bowman, Art'; 'Brenneman, Beth'; 'Brewer, Doug'; 'Buckley, John'; 'Buckley, Mark'; 'Burley, Silvia'; 'Burt, Charles'; 'Byrd, Tim'; 'Cadagan, Jerry'; 'Carlin, Michael'; 'Charles, Cindy'; 'Cismowski, Gail'; 'Colvin, Tim'; 'Costa, Jan'; 'Cowan, Jeffrey'; 'Cox, Stanley Rob'; 'Cranston, Peggy'; 'Cremeen, Rebecca'; 'Day, Kevin'; 'Day, P'; 'Denean'; 'Derwin, Maryann Moise'; Devine, John; 'Donaldson, Milford Wayne'; 'Dowd, Maggie'; 'Drekmeier, Peter'; 'Edmondson, Steve'; 'Eicher, James'; 'Fety, Lauren'; 'Findley, Timothy'; 'Fuller, Reba'; 'Furman, Donn W'; 'Ganteinbein, Julie'; 'Giglio, Deborah'; 'Gorman, Elaine'; 'Grader, Zeke'; 'Gutierrez, Monica'; 'Hackamack, Robert'; 'Hastreiter, James'; 'Hatch, Jenny'; 'Hayat, Zahra'; 'Hayden, Ann'; 'Hellam, Anita'; 'Heyne, Tim'; 'Holley, Thomas'; 'Holm, Lisa'; 'Horn, Jeff'; 'Horn, Timi'; 'Hudelson, Bill'; 'Hughes, Noah'; 'Hughes, Robert'; 'Hume, Noah'; 'Jackman, Jerry'; 'Jackson, Zac'; 'Jennings, William'; 'Jensen, Art'; 'Jensen, Laura'; 'Johannis, Mary'; 'Johnson, Brian'; 'Justin'; 'Keating, Janice'; 'Kempton, Kathryn'; 'Kinney, Teresa'; 'Koepele, Patrick'; 'Kordella, Lesley'; 'Lein, Joseph'; 'Levin, Ellen'; 'Lewis, Reggie'; 'Linkard, David'; 'Looker, Mark'; 'Lwenya, Roselynn'; 'Lyons, Bill'; 'Madden, Dan'; 'Manji, Annie'; 'Marko, Paul'; 'Marshall, Mike'; 'Martin, Michael'; 'Martin, Ramon'; 'Mathiesen, Lloyd'; 'McDaniel, Dan'; 'McDevitt, Ray'; 'McDonnell, Marty'; 'McLain, Jeffrey'; 'Means, Julie'; 'Mills, John'; 'Morningstar Pope, Rhonda'; 'Motola, Mary'; 'O'Brien, Jennifer'; 'Orvis, Tom'; 'Ott, Bob'; 'Ott, Chris'; 'Paul, Duane'; 'Pavich, Steve'; 'Pinhey, Nick'; 'Pool, Richard'; 'Porter, Ruth'; 'Powell, Melissa'; 'Puccini, Stephen'; 'Raeder, Jessie'; 'Ramirez, Tim'; 'Rea, Maria'; 'Reed, Rhonda'; 'Richardson, Kevin'; 'Ridenour, Jim'; 'Robbins, Royal'; 'Romano, David O'; 'Roos-Collins, Richard'; 'Roseman, Jesse'; 'Rothert, Steve'; 'Sandkulla, Nicole'; 'Saunders, Jenan'; 'Schutte, Allison'; 'Sears, William'; 'Shakal, Sarah'; 'Shipley, Robert'; 'Shumway, Vern'; 'Shutes, Chris'; 'Sill, Todd'; 'Slay, Ron'; 'Smith, Jim'; Staples, Rose; 'Steindorf, Dave'; 'Steiner, Dan'; 'Stone, Vicki'; 'Stork, Ron'; 'Stratton, Susan'; 'Taylor, Mary Jane'; 'Terpstra, Thomas'; 'TeVelde, George'; 'Thompson, Larry'; 'Vasquez, Sandy'; 'Verkuil, Colette'; 'Vierra, Chris'; 'Walters, Eric'; 'Wantuck, Richard'; 'Welch, Steve'; 'Wesselman, Eric'; 'Wheeler, Dan'; 'Wheeler, Dave'; 'Wheeler, Douglas'; 'Wilcox, Scott'; 'Williamson, Harry'; 'Willy, Allison'; 'Wilson, Bryan'; 'Winchell, Frank'; 'Wooster, John'; 'Workman, Michelle'; 'Yoshiyama, Ron'; 'Zipser, Wayne'
Subject: AGENDA-MATERIAL for W-AR-3 Reservoir Temp Modeling April 10 8:30 a.m.
Attachments: ReservoirModel-April2012_ModelSteps.pdf; ReservoirModelDataTable-April2012.doc; 04-10-2012_DP_ReservoirTempMtg_AGENDA.doc; MIKE_321_FM_Scientific_Doc.pdf

Please find attached four documents for the Tuesday, April 10th (8:30 am to 10:15 am) Reservoir Temperature Modeling Data and Methods Consultation Meeting (W&AR-3):

1. AGENDA
2. Reservoir Model Data Table
3. Reservoir Model Steps
4. Mike 21 and Mike 3 Flow Model FM Scientific Documentation

They will also be uploaded to the www.donpedro-relicensing.com website later today.

If you have any problems accessing this information, please let me know. Thank you.

ROSE STAPLES
CAP-OM
HDR Engineering, Inc.

Don Pedro Relicensing

Reservoir Temperature Modeling
Data and Methods Meeting (W&AR-3)

Tuesday, April 10, 2012
8:30 a.m. – 10:15 a.m.

Call-In Number 866-994-6437
Conference Code 5424697994

1. **Introductions and Background of Modelers**
2. **Overview of the Danish Hydraulic Institute and its Models**
3. **Overview of the MIKE3 Model**
4. **Model Physics and Methods**
5. **Model Input and Output; Data Sources**
6. **Schedule for Building the Model**
7. **Q&A**

MIKE 21 & MIKE 3 FLOW MODEL FM

Hydrodynamic and Transport Module

Scientific Documentation

Agern Allé 5
DK-2970 Hørsholm
Denmark

Tel: +45 4516 9200
Support: +45 4516 9333
Fax: +45 4516 9292

mikebydhi@dhigroup.com
www.mikebydhi.com

PLEASE NOTE

PRINTING HISTORY

June 2004 ..... Edition 2004

August 2005 ..... Edition 2005

April 2006 ..... Edition 2007

December 2006 ..... Edition 2007

October 2007 ..... Edition 2008

January 2009 ..... Edition 2009

February 2010 ..... Edition 2009

July 2010 ..... Edition 2011

CONTENTS

MIKE 21 & MIKE 3 FLOW MODEL FM
Hydrodynamic and Transport Module
Scientific Documentation

1 INTRODUCTION

This document presents the scientific background for the new MIKE 21 & MIKE 3 Flow Model FM[1] modelling system developed by DHI Water & Environment. The objective is to provide the user with a detailed description of the flow and transport model equations, numerical discretization and solution methods. Also model validation is discussed in this document.

MIKE 21 & MIKE 3 Flow Model FM is based on a flexible mesh approach and it has been developed for applications within oceanographic, coastal and estuarine environments. The modelling system may also be applied for studies of overland flooding.

The system is based on the numerical solution of the two/three-dimensional incompressible Reynolds averaged Navier-Stokes equations invoking the assumptions of Boussinesq and of hydrostatic pressure. Thus, the model consists of continuity, momentum, temperature, salinity and density equations and it is closed by a turbulent closure scheme. For the 3D model the free surface is taken into account using a sigma-coordinate transformation approach.

The spatial discretization of the primitive equations is performed using a cell-centred finite volume method. The spatial domain is discretized by subdivision of the continuum into non-overlapping elements/cells. In the horizontal plane an unstructured grid is used while in the vertical domain in the 3D model a structured mesh is used. In the 2D model the elements can be triangles or quadrilateral elements. In the 3D model the elements can be prisms or bricks whose horizontal faces are triangles and quadrilateral elements, respectively.

[1] Including the MIKE 21 Flow Model FM (two-dimensional flow) and MIKE 3 Flow Model FM (three-dimensional flow)

2 GOVERNING EQUATIONS

2.1 3D Governing Equations in Cartesian Co-ordinates

2.1.1 Shallow water equations

The model is based on the solution of the three-dimensional incompressible Reynolds averaged Navier-Stokes equations, subject to the assumptions of Boussinesq and of hydrostatic pressure.

The local continuity equation is written as

$$\frac{\partial u}{\partial x}+\frac{\partial v}{\partial y}+\frac{\partial w}{\partial z}=S \tag{2.1}$$

and the two horizontal momentum equations for the x- and y-component, respectively

$$\frac{\partial u}{\partial t}+\frac{\partial u^2}{\partial x}+\frac{\partial vu}{\partial y}+\frac{\partial wu}{\partial z}=fv-g\frac{\partial \eta}{\partial x}-\frac{1}{\rho_0}\frac{\partial p_a}{\partial x}- \frac{g}{\rho_0}\int_z^\eta \frac{\partial \rho}{\partial x}dz-\frac{1}{\rho_0 h}\left(\frac{\partial s_{xx}}{\partial x}+\frac{\partial s_{xy}}{\partial y}\right)+F_u+\frac{\partial}{\partial z}\left(\nu_t\frac{\partial u}{\partial z}\right)+u_sS \tag{2.2}$$

$$\frac{\partial v}{\partial t}+\frac{\partial v^2}{\partial y}+\frac{\partial uv}{\partial x}+\frac{\partial wv}{\partial z}=-fu-g\frac{\partial \eta}{\partial y}-\frac{1}{\rho_0}\frac{\partial p_a}{\partial y}- \frac{g}{\rho_0}\int_z^\eta \frac{\partial \rho}{\partial y}dz-\frac{1}{\rho_0 h}\left(\frac{\partial s_{yx}}{\partial x}+\frac{\partial s_{yy}}{\partial y}\right)+F_v+\frac{\partial}{\partial z}\left(\nu_t\frac{\partial v}{\partial z}\right)+v_sS \tag{2.3}$$

where t is the time; x, y and z are the Cartesian co-ordinates; η is the surface elevation; d is the still water depth; $h=\eta+d$ is the total water depth; u, v and w are the velocity components in the x, y and z direction; $f=2\Omega\sin\phi$ is the Coriolis parameter (Ω is the angular rate of revolution and ϕ the geographic latitude); g is the gravitational acceleration; ρ is the density of water; s_{xx}, s_{xy}, s_{yx} and s_{yy} are components of the radiation stress tensor; ν_t is the vertical turbulent (or eddy) viscosity; p_a is the atmospheric pressure; ρ_o is the reference density of water. S is the magnitude of the discharge due to point sources and (u_s, v_s) is the velocity by which the water is discharged into the ambient water. The horizontal stress terms are described using a gradient-stress relation, which is simplified to

$$F_u = \frac{\partial}{\partial x}\left(2A\frac{\partial u}{\partial x}\right) + \frac{\partial}{\partial y}\left(A\left(\frac{\partial u}{\partial y} + \frac{\partial v}{\partial x}\right)\right) \tag{2.4}$$

$$F_v = \frac{\partial}{\partial x}\left(A\left(\frac{\partial u}{\partial y} + \frac{\partial v}{\partial x}\right)\right) + \frac{\partial}{\partial y}\left(2A\frac{\partial v}{\partial y}\right) \tag{2.5}$$

where A is the horizontal eddy viscosity.

The surface and bottom boundary condition for u, v and w are

At $z = \eta$:

$$\frac{\partial \eta}{\partial t} + u\frac{\partial \eta}{\partial x} + v\frac{\partial \eta}{\partial y} - w = 0, \quad \left(\frac{\partial u}{\partial z}, \frac{\partial v}{\partial z}\right) = \frac{1}{\rho_0 \nu_t}\left(\tau_{sx}, \tau_{sy}\right) \tag{2.6}$$

At $z = -d$:

$$u\frac{\partial d}{\partial x} + v\frac{\partial d}{\partial y} + w = 0, \quad \left(\frac{\partial u}{\partial z}, \frac{\partial v}{\partial z}\right) = \frac{1}{\rho_0 \nu_t}\left(\tau_{bx}, \tau_{by}\right) \tag{2.7}$$

where $\left(\tau_{sx}, \tau_{sy}\right)$ and $\left(\tau_{bx}, \tau_{by}\right)$ are the x and y components of the surface wind and bottom stresses.

The total water depth, h, can be obtained from the kinematic boundary condition at the surface, once the velocity field is known from the momentum and continuity equations. However, a more robust equation is obtained by vertical integration of the local continuity equation

$$\frac{\partial h}{\partial t} + \frac{\partial h\bar{u}}{\partial x} + \frac{\partial h\bar{v}}{\partial y} = hS + \hat{P} - \hat{E} \tag{2.8}$$

where $\hat{P}$ and $\hat{E}$ are precipitation and evaporation rates, respectively, and $\bar{u}$ and $\bar{v}$ are the depth-averaged velocities

$$h\bar{u} = \int_{-d}^{\eta} u dz, \quad h\bar{v} = \int_{-d}^{\eta} v dz \tag{2.9}$$

The fluid is assumed to be incompressible. Hence, the density, ρ, does not depend on the pressure, but only on the temperature, T, and the salinity, s, via the equation of state

$$\rho = \rho(T, s) \tag{2.10}$$

Here the UNESCO equation of state is used (see UNESCO, 1981).

2.1.2 Transport equations for salt and temperature

The transports of temperature, T, and salinity, s, follow the general transport-diffusion equations as

$$\frac{\partial T}{\partial t}+\frac{\partial uT}{\partial x}+\frac{\partial vT}{\partial y}+\frac{\partial wT}{\partial z}=F_T+\frac{\partial}{\partial z}\left(D_v\frac{\partial T}{\partial z}\right)+\widehat{H}+T_sS \qquad (2.11)$$

$$\frac{\partial s}{\partial t}+\frac{\partial us}{\partial x}+\frac{\partial vs}{\partial y}+\frac{\partial ws}{\partial z}=F_s+\frac{\partial}{\partial z}\left(D_v\frac{\partial s}{\partial z}\right)+s_sS \qquad (2.12)$$

where D_v is the vertical turbulent (eddy) diffusion coefficient. $\widehat{H}$ is a source term due to heat exchange with the atmosphere. T_s and s_s are the temperature and the salinity of the source. F are the horizontal diffusion terms defined by

$$(F_T,F_s)=\left[\frac{\partial}{\partial x}\left(D_h\frac{\partial}{\partial x}\right)+\frac{\partial}{\partial y}\left(D_h\frac{\partial}{\partial y}\right)\right](T,s) \qquad (2.13)$$

where D_h is the horizontal diffusion coefficient. The diffusion coefficients can be related to the eddy viscosity

$$D_h=\frac{A}{\sigma_T}\quad\text{and}\quad D_v=\frac{\nu_t}{\sigma_T} \qquad (2.14)$$

where σ_T is the Prandtl number. In many applications a constant Prandtl number can be used (see Rodi (1984)).

The surface and bottom boundary conditions for the temperature are

At $z=\eta$:

$$D_h\frac{\partial T}{\partial z}=\frac{Q_n}{\rho_0c_p}+T_p\hat{P}-T_e\hat{E} \qquad (2.15)$$

At $z=-d$:

$$\frac{\partial T}{\partial z}=0 \qquad (2.16)$$

where Q_n is the surface net heat flux and $c_p = 4217\ J/(kg \cdot °K)$ is the specific heat of the water. A detailed description for determination of $\hat{H}$ and Q_n is given in Section 2.7.

The surface and bottom boundary conditions for the salinity are

At $z = \eta$:

$$\frac{\partial s}{\partial z} = 0 \tag{2.17}$$

At $z = -d$:

$$\frac{\partial s}{\partial z} = 0 \tag{2.18}$$

When heat exchange from the atmosphere is included, the evaporation is defined as

$$\hat{E} = \begin{cases} \dfrac{q_v}{\rho_0 l_v} & q_v > 0 \\ 0 & q_v \le 0 \end{cases} \tag{2.19}$$

where q_v is the latent heat flux and $l_v = 2.5 \cdot 10^6$ is the latent heat of vaporisation of water.

2.1.3 Transport equation for a scalar quantity

The conservation equation for a scalar quantity is given by

$$\frac{\partial C}{\partial t} + \frac{\partial uC}{\partial x} + \frac{\partial vC}{\partial y} + \frac{\partial wC}{\partial z} = F_C + \frac{\partial}{\partial z}\left(D_v \frac{\partial C}{\partial z} \right) - k_p C + C_s S \tag{2.20}$$

where C is the concentration of the scalar quantity, k_p is the linear decay rate of the scalar quantity, C_s is the concentration of the scalar quantity at the source and D_v is the vertical diffusion coefficient. F_F is the horizontal diffusion term defined by

$$F_C = \left[\frac{\partial}{\partial x}\left(D_h \frac{\partial}{\partial x} \right) + \frac{\partial}{\partial y}\left(D_h \frac{\partial}{\partial y} \right) \right] C \tag{2.21}$$

where D_h is the horizontal diffusion coefficient.

2.1.4 Turbulence model

The turbulence is modelled using an eddy viscosity concept. The eddy viscosity is often described separately for the vertical and the horizontal transport. Here several turbulence models can be applied: a constant viscosity, a vertically parabolic viscosity and a standard k-ε model (Rodi, 1984). In many numerical simulations the small-scale turbulence can not be resolved with the chosen spatial resolution. This kind of turbulence can be approximated using sub-grid scale models.

Vertical eddy viscosity

The eddy viscosity derived from the log-law is calculated by

$$\nu_t = U_\tau h\left(c_1\frac{z+d}{h} + c_2\left(\frac{z+d}{h}\right)^2\right) \tag{2.22}$$

where $U_\tau = \max(U_{\tau s}, U_{\tau b})$ and c_1 and c_2 are two constants. $U_{\tau s}$ and $U_{\tau b}$ are the friction velocities associated with the surface and bottom stresses, $c_1 = 0.41$ and $c_2 = -0.41$ give the standard parabolic profile.

In applications with stratification the effects of buoyancy can be included explicitly. This is done through the introduction of a Richardson number dependent damping of the eddy viscosity coefficient, when a stable stratification occurs. The damping is a generalisation of the Munk-Anderson formulation (Munk and Anderson, 1948)

$$\nu_t = \nu_t^*(1 + aRi)^{-b} \tag{2.23}$$

where ν_t^* is the undamped eddy viscosity and *Ri* is the local gradient Richardson number

$$Ri = -\frac{g}{\rho_0}\frac{\partial\rho}{\partial z}\left(\left(\frac{\partial u}{\partial z}\right)^2 + \left(\frac{\partial v}{\partial z}\right)^2\right)^{-1} \tag{2.24}$$

$a = 10$ and $b = 0.5$ are empirical constants.

In the k-ε model the eddy-viscosity is derived from turbulence parameters k and ε as

$$\nu_t = c_\mu\frac{k^2}{\varepsilon} \tag{2.25}$$

where k is the turbulent kinetic energy per unit mass (TKE), ε is the dissipation of TKE and c_μ is an empirical constant.

The turbulent kinetic energy, k, and the dissipation of TKE, ε, are obtained from the following transport equations

$$\frac{\partial k}{\partial t}+\frac{\partial uk}{\partial x}+\frac{\partial vk}{\partial y}+\frac{\partial wk}{\partial z}=F_k+\frac{\partial}{\partial z}\left(\frac{\nu_t}{\sigma_k}\frac{\partial k}{\partial z}\right)+P+B-\varepsilon \tag{2.26}$$

$$\frac{\partial \varepsilon}{\partial t}+\frac{\partial u\varepsilon}{\partial x}+\frac{\partial v\varepsilon}{\partial y}+\frac{\partial w\varepsilon}{\partial z}= F_\varepsilon+\frac{\partial}{\partial z}\left(\frac{\nu_t}{\sigma_\varepsilon}\frac{\partial \varepsilon}{\partial z}\right)+\frac{\varepsilon}{k}\left(c_{1\varepsilon}P+c_{3\varepsilon}B-c_{2\varepsilon}\varepsilon\right) \tag{2.27}$$

where the shear production, P, and the buoyancy production, B, are given as

$$P=\frac{\tau_{xz}}{\rho_0}\frac{\partial u}{\partial z}+\frac{\tau_{yz}}{\rho_0}\frac{\partial v}{\partial z}\approx \nu_t\left(\left(\frac{\partial u}{\partial z}\right)^2+\left(\frac{\partial v}{\partial z}\right)^2\right) \tag{2.28}$$

$$B=-\frac{\nu_t}{\sigma_t}N^2 \tag{2.29}$$

with the Brunt-Väisälä frequency, N, defined by

$$N^2=-\frac{g}{\rho_0}\frac{\partial \rho}{\partial z} \tag{2.30}$$

σ_t is the turbulent Prandtl number and σ_k, σ_ε, $c_{1\varepsilon}$, $c_{2\varepsilon}$ and $c_{3\varepsilon}$ are empirical constants. F are the horizontal diffusion terms defined by

$$(F_k,F_\varepsilon)=\left[\frac{\partial}{\partial x}\left(D_h\frac{\partial}{\partial x}\right)+\frac{\partial}{\partial y}\left(D_h\frac{\partial}{\partial y}\right)\right](k,\varepsilon) \tag{2.31}$$

The horizontal diffusion coefficients are given by $D_h=A/\sigma_k$ and $D_h=A/\sigma_\varepsilon$, respectively.

Several carefully calibrated empirical coefficients enter the k-e turbulence model. The empirical constants are listed in (2.47) (see Rodi, 1984).

Table 2.1 Empirical constants in the k-ε model.

c_μ	$c_{1\varepsilon}$	$c_{2\varepsilon}$	$c_{3\varepsilon}$	σ_t	σ_k	σ_ε
0.09	1.44	1.92	0	0.9	1.0	1.3

At the surface the boundary conditions for the turbulent kinetic energy and its rate of dissipation depend on the wind shear, $U_{\tau s}$

At $z = \eta$:

$$k = \frac{1}{\sqrt{c_\mu}} U_{\tau s}^2 \tag{2.32}$$

$$\varepsilon = \frac{U_{\tau s}^3}{\kappa \Delta z_b} \qquad \text{for} \quad U_{\tau s} > 0$$

$$\frac{\partial k}{\partial z} = 0 \qquad \varepsilon = \frac{\left(k\sqrt{c_\mu}\right)^{3/2}}{a\kappa h} \qquad \text{for} \quad U_{\tau s} = 0 \tag{2.33}$$

where κ =0.4 is the von Kármán constant, $a = 0.07$ is and empirical constant and Δz_s is the distance from the surface where the boundary condition is imposed. At the seabed the boundary conditions are

At $z = -d$:

$$k = \frac{1}{\sqrt{c_\mu}} U_{\tau b}^2 \qquad \varepsilon = \frac{U_{\tau b}^3}{\kappa \Delta z_b} \tag{2.34}$$

where Δz_b is the distance from the bottom where the boundary condition is imposed.

Horizontal eddy viscosity

In many applications a constant eddy viscosity can be used for the horizontal eddy viscosity. Alternatively, Smagorinsky (1963) proposed to express sub-grid scale transports by an effective eddy viscosity related to a characteristic length scale. The subgrid scale eddy viscosity is given by

$$A = c_s^2 l^2 \sqrt{2 S_{ij} S_{ij}} \tag{2.35}$$

where c_s is a constant, l is a characteristic length and the deformation rate is given by

$$S_{ij} = \frac{1}{2}\left(\frac{\partial u_i}{\partial x_j} + \frac{\partial u_j}{\partial x_i}\right) \quad (i,j = 1,2) \tag{2.36}$$

2.1.5 Governing equations in Cartesian and sigma-co-ordinates

The equations are solved using a vertical σ-transformation

$$\sigma = \frac{z - z_b}{h}, \quad x' = x, \quad y' = y \tag{2.37}$$

where σ varies between 0 at the bottom and 1 at the surface. The co-ordinate transformation implies relations such as

$$\frac{\partial}{\partial z} = \frac{1}{h}\frac{\partial}{\partial \sigma} \tag{2.38}$$

$$\left(\frac{\partial}{\partial x}, \frac{\partial}{\partial y}\right) = \left(\frac{\partial}{\partial x'} - \frac{1}{h}\left(-\frac{\partial d}{\partial x} + \sigma\frac{\partial h}{\partial x}\right)\frac{\partial}{\partial \sigma}, \frac{\partial}{\partial y'} - \frac{1}{h}\left(-\frac{\partial d}{\partial y} + \sigma\frac{\partial h}{\partial y}\right)\frac{\partial}{\partial \sigma}\right) \tag{2.39}$$

In this new co-ordinate system the governing equations are given as

$$\frac{\partial h}{\partial t} + \frac{\partial hu}{\partial x'} + \frac{\partial hv}{\partial y'} + \frac{\partial h\omega}{\partial \sigma} = hS \tag{2.40}$$

$$\begin{aligned}\frac{\partial hu}{\partial t} + \frac{\partial hu^2}{\partial x'} + \frac{\partial hvu}{\partial y'} + \frac{\partial h\omega u}{\partial \sigma} = {} & fvh - gh\frac{\partial \eta}{\partial x'} - \frac{h}{\rho_0}\frac{\partial p_a}{\partial x'} - \\ & \frac{hg}{\rho_0}\int_z^\eta \frac{\partial \rho}{\partial x}dz - \frac{1}{\rho_0}\left(\frac{\partial s_{xx}}{\partial x} + \frac{\partial s_{xy}}{\partial y}\right) + hF_u + \frac{\partial}{\partial \sigma}\left(\frac{\nu_v}{h}\frac{\partial u}{\partial \sigma}\right) + hu_s S\end{aligned} \tag{2.41}$$

$$\begin{aligned}\frac{\partial hv}{\partial t} + \frac{\partial huv}{\partial x'} + \frac{\partial hv^2}{\partial y'} + \frac{\partial h\omega v}{\partial \sigma} = {} & -fuh - gh\frac{\partial \eta}{\partial y'} - \frac{h}{\rho_0}\frac{\partial p_a}{\partial y'} - \\ & \frac{hg}{\rho_0}\int_z^\eta \frac{\partial \rho}{\partial y}dz - \frac{1}{\rho_0}\left(\frac{\partial s_{yx}}{\partial x} + \frac{\partial s_{yy}}{\partial y}\right) + hF_v + \frac{\partial}{\partial \sigma}\left(\frac{\nu_v}{h}\frac{\partial v}{\partial \sigma}\right) + hv_s S\end{aligned} \tag{2.42}$$

$$\begin{aligned}\frac{\partial hT}{\partial t} + \frac{\partial huT}{\partial x'} + \frac{\partial hvT}{\partial y'} + \frac{\partial h\omega T}{\partial \sigma} = {} & \\ & hF_T + \frac{\partial}{\partial \sigma}\left(\frac{D_v}{h}\frac{\partial T}{\partial \sigma}\right) + h\tilde{H} + hT_s S\end{aligned} \tag{2.43}$$

$$\frac{\partial hs}{\partial t} + \frac{\partial hus}{\partial x'} + \frac{\partial hvs}{\partial y'} + \frac{\partial h\omega s}{\partial \sigma} = hF_s + \frac{\partial}{\partial \sigma}\left(\frac{D_v}{h}\frac{\partial s}{\partial \sigma}\right) + hs_s S \tag{2.44}$$

$$\frac{\partial hk}{\partial t}+\frac{\partial huk}{\partial x'}+\frac{\partial hvk}{\partial y'}+\frac{\partial h\omega k}{\partial \sigma}= hF_k+\frac{1}{h}\frac{\partial}{\partial \sigma}\left(\frac{\nu_t}{\sigma_k}\frac{\partial k}{\partial \sigma}\right)+h(P+B-\varepsilon) \tag{2.45}$$

$$\frac{\partial h\varepsilon}{\partial t}+\frac{\partial hu\varepsilon}{\partial x'}+\frac{\partial hv\varepsilon}{\partial y'}+\frac{\partial h\omega\varepsilon}{\partial \sigma}= hF_\varepsilon+\frac{1}{h}\frac{\partial}{\partial \sigma}\left(\frac{\nu_t}{\sigma_\varepsilon}\frac{\partial \varepsilon}{\partial \sigma}\right)+h\frac{\varepsilon}{k}\left(c_{1\varepsilon}P+c_{3\varepsilon}B-c_{2\varepsilon}\varepsilon\right) \tag{2.46}$$

$$\frac{\partial hC}{\partial t}+\frac{\partial huC}{\partial x'}+\frac{\partial hvC}{\partial y'}+\frac{\partial h\omega C}{\partial \sigma}=hF_C+\frac{\partial}{\partial \sigma}\left(\frac{D_v}{h}\frac{\partial C}{\partial \sigma}\right)-hk_pC+hC_s \tag{2.47}$$

The modified vertical velocity is defined by

$$\omega=\frac{1}{h}\left[w+u\frac{\partial d}{\partial x'}+v\frac{\partial d}{\partial y'}-\sigma\left(\frac{\partial h}{\partial t}+u\frac{\partial h}{\partial x'}+v\frac{\partial h}{\partial y'}\right)\right] \tag{2.48}$$

The modified vertical velocity is the velocity across a level of constant σ. The horizontal diffusion terms are defined as

$$hF_u\approx\frac{\partial}{\partial x}\left(2hA\frac{\partial u}{\partial x}\right)+\frac{\partial}{\partial y}\left(hA\left(\frac{\partial u}{\partial y}+\frac{\partial v}{\partial x}\right)\right) \tag{2.49}$$

$$hF_v\approx\frac{\partial}{\partial x}\left(hA\left(\frac{\partial u}{\partial y}+\frac{\partial v}{\partial x}\right)\right)+\frac{\partial}{\partial y}\left(2hA\frac{\partial v}{\partial y}\right) \tag{2.50}$$

$$h(F_T,F_s,F_k,F_\varepsilon,F_c)\approx\left[\frac{\partial}{\partial x}\left(hD_h\frac{\partial}{\partial x}\right)+\frac{\partial}{\partial y}\left(hD_h\frac{\partial}{\partial y}\right)\right](T,s,k,\varepsilon,C) \tag{2.51}$$

The boundary condition at the free surface and at the bottom are given as follows

At σ=1:

$$\omega=0,\quad\left(\frac{\partial u}{\partial \sigma},\frac{\partial v}{\partial \sigma}\right)=\frac{h}{\rho_0\nu_t}\left(\tau_{sx},\tau_{sy}\right) \tag{2.52}$$

At σ=0:

(2.53)

$$\omega = 0, \quad \left(\frac{\partial u}{\partial \sigma}, \frac{\partial v}{\partial \sigma}\right) = \frac{h}{\rho_0 \nu_t}\left(\tau_{bx}, \tau_{by}\right)$$

The equation for determination of the water depth is not changed by the co-ordinate transformation. Hence, it is identical to Eq. (2.6).

2.2 3D Governing Equations in Spherical and Sigma Co-ordinates

In spherical co-ordinates the independent variables are the longitude, λ, and the latitude, ϕ. The horizontal velocity field (u,v) is defined by

$$u = R\cos\phi\frac{d\lambda}{dt} \qquad v = R\frac{d\phi}{dt} \tag{2.54}$$

where R is the radius of the earth.

In this co-ordinate system the governing equations are given as (all superscripts indicating the horizontal co-ordinate in the new co-ordinate system are dropped in the following for notational convenience)

$$\frac{\partial h}{\partial t} + \frac{1}{R\cos\phi}\left(\frac{\partial hu}{\partial \lambda} + \frac{\partial hv\cos\phi}{\partial \phi}\right) + \frac{\partial h\omega}{\partial \sigma} = hS \tag{2.55}$$

$$\begin{aligned}\frac{\partial hu}{\partial t} + \frac{1}{R\cos\phi}\left(\frac{\partial hu^2}{\partial \lambda} + \frac{\partial hvu\cos\phi}{\partial \phi}\right) + \frac{\partial h\omega u}{\partial \sigma} = \left(f + \frac{u}{R}\tan\phi\right)vh - \\ \frac{1}{R\cos\phi}\left(gh\frac{\partial \eta}{\partial \lambda} + \frac{1}{\rho_0}\frac{\partial p_a}{\partial \lambda} + \frac{g}{\rho_0}\int_z^\eta \frac{\partial \rho}{\partial \lambda}dz + \frac{1}{\rho_0}\left(\frac{\partial s_{xx}}{\partial \lambda} + \cos\phi\frac{\partial s_{xy}}{\partial \phi}\right)\right) + \\ hF_u + \frac{\partial}{\partial \sigma}\left(\frac{\nu_v}{h}\frac{\partial u}{\partial \sigma}\right) + hu_s S\end{aligned} \tag{2.56}$$

$$\begin{aligned}\frac{\partial hv}{\partial t} + \frac{1}{R\cos\phi}\left(\frac{\partial huv}{\partial \lambda} + \frac{\partial hv^2\cos\phi}{\partial \phi}\right) + \frac{\partial h\omega v}{\partial \sigma} = -\left(f + \frac{u}{R}\tan\phi\right)uh - \\ \frac{1}{R}\left(gh\frac{\partial \eta}{\partial \phi} + \frac{1}{\rho_0}\frac{\partial p_a}{\partial \phi} + \frac{g}{\rho_0}\int_z^\eta \frac{\partial \rho}{\partial \phi}dz + \frac{1}{\rho_0}\left(\frac{1}{\cos\phi}\frac{\partial s_{yx}}{\partial \lambda} + \frac{\partial s_{yy}}{\partial \phi}\right)\right) + \\ hF_v + \frac{\partial}{\partial \sigma}\left(\frac{\nu_v}{h}\frac{\partial v}{\partial \sigma}\right) + hv_s S\end{aligned} \tag{2.57}$$

$$\begin{aligned}\frac{\partial hT}{\partial t} + \frac{1}{R\cos\phi}\left(\frac{\partial huT}{\partial \lambda} + \frac{\partial hvT\cos\phi}{\partial \phi}\right) + \frac{\partial h\omega T}{\partial \sigma} = \\ hF_T + \frac{\partial}{\partial \sigma}\left(\frac{D_v}{h}\frac{\partial T}{\partial \sigma}\right) + h\widehat{H} + hT_s S\end{aligned} \tag{2.58}$$

$$\frac{\partial hs}{\partial t}+\frac{1}{R\cos\phi}\left(\frac{\partial hus}{\partial\lambda}+\frac{\partial hvs\cos\phi}{\partial\phi}\right)+\frac{\partial h\omega s}{\partial\sigma}= hF_s+\frac{\partial}{\partial\sigma}\left(\frac{D_v}{h}\frac{\partial s}{\partial\sigma}\right)+hs_sS \tag{2.59}$$

$$\frac{\partial hk}{\partial t}+\frac{1}{R\cos\phi}\left(\frac{\partial huk}{\partial\lambda}+\frac{\partial hvk\cos\phi}{\partial\phi}\right)+\frac{\partial h\omega k}{\partial\sigma}= hF_k+\frac{1}{h}\frac{\partial}{\partial\sigma}\left(\frac{\nu_t}{\sigma_k}\frac{\partial k}{\partial\sigma}\right)+h(P+B-\varepsilon) \tag{2.60}$$

$$\frac{\partial h\varepsilon}{\partial t}+\frac{1}{R\cos\phi}\left(\frac{\partial hu\varepsilon}{\partial\lambda}+\frac{\partial hv\varepsilon\cos\phi}{\partial\phi}\right)+\frac{\partial h\omega\varepsilon}{\partial\sigma}= hF_\varepsilon+\frac{1}{h}\frac{\partial}{\partial\sigma}\left(\frac{\nu_t}{\sigma_\varepsilon}\frac{\partial\varepsilon}{\partial\sigma}\right)+h\frac{\varepsilon}{k}\left(c_{1\varepsilon}P+c_{3\varepsilon}B-c_{2\varepsilon}\varepsilon\right) \tag{2.61}$$

$$\frac{\partial hC}{\partial t}+\frac{1}{R\cos\phi}\left(\frac{\partial huC}{\partial\lambda}+\frac{\partial hvC\cos\phi}{\partial\phi}\right)+\frac{\partial h\omega C}{\partial\sigma}= hF_C+\frac{\partial}{\partial\sigma}\left(\frac{D_v}{h}\frac{\partial C}{\partial\sigma}\right)-hk_pC+hC_sS \tag{2.62}$$

The modified vertical velocity in spherical co-ordinates is defined by

$$\omega=\frac{1}{h}\left[w+\frac{u}{R\cos\phi}\frac{\partial d}{\partial\lambda}+\frac{v}{R}\frac{\partial d}{\partial y}-\sigma\left(\frac{\partial h}{\partial t}+\frac{u}{R\cos\phi}\frac{\partial h}{\partial\lambda}+\frac{v}{R}\frac{\partial h}{\partial\phi}\right)\right] \tag{2.63}$$

The equation determining the water depth in spherical co-ordinates is given as

$$\frac{\partial h}{\partial t}+\frac{1}{R\cos\phi}\left(\frac{\partial h\bar{u}}{\partial\lambda}+\frac{\partial h\bar{v}\cos\phi}{\partial\phi}\right)=hS \tag{2.64}$$

2.3 2D Governing Equations in Cartesian Co-ordinates

2.3.1 Shallow water equations

Integration of the horizontal momentum equations and the continuity equation over depth $h=\eta+d$ the following two-dimensional shallow water equations are obtained

$$\frac{\partial h}{\partial t}+\frac{\partial h\bar{u}}{\partial x}+\frac{\partial h\bar{v}}{\partial y}=hS \tag{2.65}$$

$$\frac{\partial h\bar{u}}{\partial t}+\frac{\partial h\bar{u}^2}{\partial x}+\frac{\partial h\bar{v}\bar{u}}{\partial y}=f\bar{v}h-gh\frac{\partial \eta}{\partial x}-\frac{h}{\rho_0}\frac{\partial p_a}{\partial x}-\frac{gh^2}{2\rho_0}\frac{\partial \rho}{\partial x}+\frac{\tau_{sx}}{\rho_0}-\frac{\tau_{bx}}{\rho_0}-\frac{1}{\rho_0}\left(\frac{\partial s_{xx}}{\partial x}+\frac{\partial s_{xy}}{\partial y}\right)+\frac{\partial}{\partial x}\left(hT_{xx}\right)+\frac{\partial}{\partial y}\left(hT_{xy}\right)+hu_sS \quad (2.66)$$

$$\frac{\partial h\bar{v}}{\partial t}+\frac{\partial h\bar{u}\bar{v}}{\partial x}+\frac{\partial h\bar{v}^2}{\partial y}=-f\bar{u}h-gh\frac{\partial \eta}{\partial y}-\frac{h}{\rho_0}\frac{\partial p_a}{\partial y}-\frac{gh^2}{2\rho_0}\frac{\partial \rho}{\partial y}+\frac{\tau_{sy}}{\rho_0}-\frac{\tau_{by}}{\rho_0}-\frac{1}{\rho_0}\left(\frac{\partial s_{yx}}{\partial x}+\frac{\partial s_{yy}}{\partial y}\right)+\frac{\partial}{\partial x}\left(hT_{xy}\right)+\frac{\partial}{\partial y}\left(hT_{yy}\right)+hv_sS \quad (2.67)$$

The overbar indicates a depth average value. For example, $\bar{u}$ and $\bar{v}$ are the depth-averaged velocities defined by

$$h\bar{u}=\int_{-d}^{\eta}u\,dz\,,\quad h\bar{v}=\int_{-d}^{\eta}v\,dz \quad (2.68)$$

The lateral stresses T_{ij} include viscous friction, turbulent friction and differential advection. They are estimated using an eddy viscosity formulation based on of the depth average velocity gradients

$$T_{xx}=2A\frac{\partial \bar{u}}{\partial x},\quad T_{xy}=A\left(\frac{\partial \bar{u}}{\partial y}+\frac{\partial \bar{v}}{\partial x}\right),\quad T_{yy}=2A\frac{\partial \bar{v}}{\partial y} \quad (2.69)$$

2.3.2 Transport equations for salt and temperature

Integrating the transport equations for salt and temperature over depth the following two-dimensional transport equations are obtained

$$\frac{\partial h\bar{T}}{\partial t}+\frac{\partial h\bar{u}\bar{T}}{\partial x}+\frac{\partial h\bar{v}\bar{T}}{\partial y}=hF_T+h\hat{H}+hT_sS \quad (2.70)$$

$$\frac{\partial h\bar{s}}{\partial t}+\frac{\partial h\bar{u}\bar{s}}{\partial x}+\frac{\partial h\bar{v}\bar{s}}{\partial y}=hF_s+hs_sS \quad (2.71)$$

where $\bar{T}$ and $\bar{s}$ is the depth average temperature and salinity.

2.3.3 Transport equations for a scalar quantity

Integrating the transport equations for a scalar quantity over depth the following two-dimensional transport equations are obtained

$$\frac{\partial h\overline{C}}{\partial t}+\frac{\partial h\overline{u}\,\overline{C}}{\partial x}+\frac{\partial h\overline{v}\,\overline{C}}{\partial y}=hF_C-hk_p\overline{C}+hC_sS \tag{2.72}$$

where $\overline{C}$ is the depth average scalar quantity.

2.4 2D Governing Equations in Spherical Co-ordinates

In spherical co-ordinates the independent variables are the longitude, λ ,and the latitude, ϕ . The horizontal velocity field (u,v) is defined by

$$\overline{u}=R\cos\phi\frac{d\lambda}{dt}\qquad\qquad\overline{v}=R\frac{d\phi}{dt} \tag{2.73}$$

where R is the radius of the earth.

In spherical co-ordinates the governing equation can be written

$$\frac{\partial h}{\partial t}+\frac{1}{R\cos\phi}\left(\frac{\partial h\overline{u}}{\partial\lambda}+\frac{\partial h\overline{v}\cos\phi}{\partial\phi}\right)=0 \tag{2.74}$$

$$\begin{aligned}&\frac{\partial h\overline{u}}{\partial t}+\frac{1}{R\cos\phi}\left(\frac{\partial h\overline{u}^2}{\partial\lambda}+\frac{\partial h\overline{v}\overline{u}\cos\phi}{\partial\phi}\right)=\left(f+\frac{\overline{u}}{R}\tan\phi\right)\overline{v}h\\&-\frac{1}{R\cos\phi}\left(gh\frac{\partial\eta}{\partial\lambda}-\frac{h}{\rho_0}\frac{\partial p_a}{\partial\lambda}+\frac{gh^2}{2\rho_0}\frac{\partial\rho}{\partial\lambda}+\frac{1}{\rho_0}\left(\frac{\partial s_{xx}}{\partial\lambda}+\cos\phi\frac{\partial s_{xy}}{\partial\phi}\right)\right)+\\&\frac{\tau_{sx}}{\rho_0}-\frac{\tau_{bx}}{\rho_0}+\frac{\partial}{\partial x}\left(hT_{xx}\right)+\frac{\partial}{\partial y}\left(hT_{xy}\right)+hu_sS\end{aligned} \tag{2.75}$$

$$\begin{aligned}&\frac{\partial h\overline{v}}{\partial t}+\frac{1}{R\cos\phi}\left(\frac{\partial h\overline{u}\overline{v}}{\partial\lambda}+\frac{\partial h\overline{v}^2\cos\varphi}{\partial\iota}\right)=-\left(f+\frac{\overline{u}}{R}\tan\phi\right)\overline{u}h\\&-\frac{1}{R}\left(gh\frac{\partial\eta}{\partial\phi}-\frac{h}{\rho_0}\frac{\partial p_a}{\partial\phi}+\frac{gh^2}{2\rho_0}\frac{\partial\rho}{\partial\phi}+\frac{1}{\rho_0}\left(\frac{1}{\cos\phi}\frac{\partial s_{yx}}{\partial\lambda}+\frac{\partial s_{yy}}{\partial\phi}\right)\right)+\\&\frac{\tau_{sy}}{\rho_0}-\frac{\tau_{by}}{\rho_0}+\frac{\partial}{\partial x}\left(hT_{xy}\right)+\frac{\partial}{\partial y}\left(hT_{yy}\right)+hv_sS\end{aligned} \tag{2.76}$$

$$\frac{\partial h\overline{T}}{\partial t}+\frac{1}{R\cos\phi}\left(\frac{\partial h\overline{u}\,\overline{T}}{\partial\lambda}+\frac{\partial h\overline{v}\,\overline{T}\cos\phi}{\partial\phi}\right)=hF_T+h\widehat{H}+hT_sS \tag{2.77}$$

$$\frac{\partial h\overline{s}}{\partial t}+\frac{1}{R\cos\phi}\left(\frac{\partial h\overline{u}\overline{s}}{\partial \lambda}+\frac{\partial h\overline{v}\overline{s}\cos\phi}{\partial \phi}\right)=hF_s+hs_sS \tag{2.78}$$

$$\frac{\partial h\overline{C}}{\partial t}+\frac{1}{R\cos\phi}\left(\frac{\partial h\overline{u}\overline{C}}{\partial \lambda}+\frac{\partial h\overline{v}\overline{C}\cos\phi}{\partial \phi}\right)=hF_C-hk_p\overline{C}+hC_sS \tag{2.79}$$

2.5 Bottom Stress

The bottom stress, $\vec{\tau}_b=(\tau_{bx},\tau_{by})$, is determined by a quadratic friction law

$$\frac{\vec{\tau}_b}{\rho_0}=c_f\vec{u}_b|\vec{u}_b| \tag{2.80}$$

where c_f is the drag coefficient and $\vec{u}_b=(u_b,v_b)$ is the flow velocity above the bottom. The friction velocity associated with the bottom stress is given by

$$U_{\tau b}=\sqrt{c_f|u_b|^2} \tag{2.81}$$

For two-dimensional calculations $\vec{u}_b$ is the depth-average velocity and the drag coefficient can be determined from the Chezy number, C, or the Manning number, M

$$c_f=\frac{g}{C^2} \tag{2.82}$$

$$c_f=\frac{g}{\left(Mh^{1/6}\right)^2} \tag{2.83}$$

For three-dimensional calculations $\vec{u}_b$ is the velocity at a distance Δz_b above the sea bed and the drag coefficient is determined by assuming a logarithmic profile between the seabed and a point Δz_b above the seabed

$$c_f=\frac{1}{\left(\frac{1}{\kappa}\ln\left(\frac{\Delta z_b}{z_0}\right)\right)^2} \tag{2.84}$$

where κ =0.4 is the von Kármán constant and z_0 is the bed roughness length scale. When the boundary surface is rough, z_0, depends on the roughness height, k_s

$$z_0 = mk_s \tag{2.85}$$

where m is approximately 1/30.

Note, that the Manning number can be estimated from the bed roughness length using the following

$$M = \frac{25.4}{k_s^{1/6}} \tag{2.86}$$

2.6 Wind Stress

In areas not covered by ice the surface stress, $\vec{\tau}_s = (\tau_{sx}, \tau_{sy})$, is determined by the winds above the surface. The stress is given by the following empirical relation

$$\bar{\tau}_s = \rho_a c_d |u_w| \bar{u}_w \tag{2.87}$$

where ρ_a is the density of air, c_d is the drag coefficient of air, and $\vec{u}_w = (u_w, v_w)$ is the wind speed 10 m above the sea surface. The friction velocity associated with the surface stress is given by

$$U_{\tau s} = \sqrt{\frac{\rho_a c_f |\bar{u}_w|^2}{\rho_0}} \tag{2.88}$$

The drag coefficient can either be a constant value or depend on the wind speed. The empirical formula proposed by Wu (1980, 1994) is used for the parameterisation of the drag coefficient.

$$c_f = \begin{cases} c_a & w_{10} < w_a \\ c_a + \dfrac{c_b - c_a}{w_b - w_a}(w_{10} - w_a) & w_a \le w_{10} < w_b \\ c_b & w_{10} \ge w_b \end{cases} \tag{2.89}$$

where c_a, c_b, w_a and w_b are empirical factors and w_{10} is the wind velocity 10 m above the sea surface. The default values for the empirical factors are $c_a = 1.255 \cdot 10^{-3}$, $c_b = 2.425 \cdot 10^{-3}$, $w_a = 7$ m/s and $w_b = 25$ m/s. These give generally good results for open sea applications. Field measurements of the drag coefficient collected over

lakes indicate that the drag coefficient is larger than open ocean data. For a detailed description of the drag coefficient see Geernaert and Plant (1990).

2.7 Ice Coverage

It is possible to take into account the effects of ice coverage on the flow field.

In areas where the sea is covered by ice the wind stress is excluded. Instead, the surface stress is caused by the ice roughness. The surface stress, $\vec{\tau}_s = (\tau_{sx}, \tau_{sy})$, is determined by a quadratic friction law

$$\frac{\vec{\tau}_s}{\rho_0} = c_f \vec{u}_s |\vec{u}_s| \tag{2.90}$$

where c_f is the drag coefficient and $\vec{u}_s = (u_s, v_s)$ is the flow velocity below the surface. The friction velocity associated with the surface stress is given by

$$U_{\tau s} = \sqrt{c_f |u_s|^2} \tag{2.91}$$

For two-dimensional calculations $\vec{u}_s$ is the depth-average velocity and the drag coefficient can be determined from the Manning number, M

$$c_f = \frac{g}{\left(Mh^{1/6}\right)^2} \tag{2.92}$$

The Manning number is estimated from the bed roughness length using the following

$$M = \frac{25.4}{k_s^{1/6}} \tag{2.93}$$

For three-dimensional calculations $\vec{u}_s$ is the velocity at a distance Δz_s below the surface and the drag coefficient is determined by assuming a logarithmic profile between the surface and a point Δz_b below the surface

$$c_f = \frac{1}{\left(\frac{1}{\kappa}\ln\left(\frac{\Delta z_s}{z_0}\right)\right)^2} \tag{2.94}$$

where κ =0.4 is the von Kármán constant and z_0 is the bed roughness length scale. When the boundary surface is rough, z_0 , depends on the roughness height, k_s

$$z_0 = mk_s \tag{2.95}$$

where m is approximately 1/30.

2.8 Tidal Potential

The tidal potential is a force, generated by the variations in gravity due to the relative motion of the earth, the moon and the sun that act throughout the computational domain. The forcing is expanded in frequency space and the potential considered as the sum of a number of terms each representing different tidal constituents. The forcing is implemented as a so-called equilibrium tide, which can be seen as the elevation that theoretically would occur, provided the earth was covered with water. The forcing enters the momentum equations (e.g. (2.66) or (2.75)) as an additional term representing the gradient of the equilibrium tidal elevations, such that the elevation η can be seen as the sum of the actual elevation and the equilibrium tidal potential.

$$\eta = \eta_{ACTUAL} + \eta_T \tag{2.96}$$

The equilibrium tidal potential η_T is given as

$$\eta_T = \sum_i e_i H_i f_i L_i \cos(2\pi \frac{t}{T_i} + b_i + i_0 x) \tag{2.97}$$

where η_T is the equilibrium tidal potential, i refers to constituent number (note that the constituents here are numbered sequentially), e_i is a correction for earth tides based on Love numbers, H_i is the amplitude, f_i is a nodal factor, L_i is given below, t is time, T_i is the period of the constituent, b_i is the phase and x is the longitude of the actual position.

The phase b is based on the motion of the moon and the sun relative to the earth and can be given by

$$b_i = (i_1 - i_0)s + (i_2 + i_0)h + i_3 p + i_4 N + i_5 p_s + u_i \sin(N) \tag{2.98}$$

where i_0 is the species, i_1 to i_5 are Doodson numbers, u is a nodal modulation factor (see Table 2.3) and the astronomical arguments s, h, p, N and p_s are given in Table 2.2.

Table 2.2 Astronomical arguments (Pugh, 1987)

Mean longitude of the moon	s	$277.02+481267.89T+0.0011T^2$
Mean longitude of the sun	h	$280.19+36000.77T+0.0003T^2$
Longitude of lunar perigee	p	$334.39+4069.04T+0.0103T^2$
Longitude of lunar ascending node	N	$259.16+1934.14T+0.0021T^2$
Longitude of perihelion	p_s	$281.22+1.72T+0.0005T^2$

In Table 2.2 the time, T, is in Julian century from January 1 1900 UTC, thus $T = (365(y - 1900) + (d - 1) + i)/36525$ and $i = int\ (y-1901)/4)$, y is year and d is day number

L depends on species number i_0 and latitude y as

$$i_0 = 0 \qquad L = 3\sin^2(y) - 1$$
$$i_0 = 1 \qquad L = \sin(2y)$$
$$i_0 = 2 \qquad L = \cos^2(y)$$

The nodal factor f_i represents modulations to the harmonic analysis and can for some constituents be given as shown in Table 2.3.

Table 2.3 Nodal modulation terms (Pugh, 1987)

	f_i	u_i
M_m	1.000 - 0.130 cos(N)	0
M_f	1.043 + 0.414 cos(N)	-23.7 sin(N)
Q_1, O_1	1.009 + 0.187 cos(N)	10.8 sin(N)
K_1	1.006 + 0.115 cos(N)	-8.9 sin(N)
$2N_2$, μ_2, ν_2, N_2, M_2	1.000 + 0.037 cos(N)	-2.1 sin(N)
K_2	1.024 + 0.286 cos(N)	-17.7 sin(N)

2.9 Wave Radiation

The second order stresses due to breaking of short period waves can be included in the simulation. The radiation stresses act as driving forces for the mean flow and can be used to calculate wave induced flow. For 3D simulations a simple approach is used. Here a uniform variation is used for the vertical variation in radiation stress.

2.10 Heat Exchange

The heat exchange with the atmosphere is calculated on basis of the four physical processes

- Latent heat flux (or the heat loss due to vaporisation)
- Sensible heat flux (or the heat flux due to convection)
- Net short wave radiation
- Net long wave radiation

Latent and sensible heat fluxes and long-wave radiation are assumed to occur at the surface. The absorption profile for the short-wave flux is approximated using Beer's law. The attenuation of the light intensity is described through the modified Beer's law as

$$I(d) = (1-\beta) I_0 e^{-\lambda d} \tag{2.99}$$

where $I(d)$ is the intensity at depth d below the surface; I_0 is the intensity just below the water surface; β is a quantity that takes into account that a fraction of light energy (the infrared) is absorbed near the surface; λ is the light extinction coefficient. Typical values for β and λ are 0.2-0.6 and 0.5-1.4 m^{04}, respectively. β and λ are user-specified constants. The default values are $\beta = 0.3$ and $\lambda = 1.0\ m^{-1}$. The fraction of the light energy that is absorbed near the surface is βI_0. The net short-wave radiation, $q_{sr,net}$, is attenuated as described by the modified Beer's law. Hence the surface net heat flux is given by

$$Q_n = q_v + q_c + \beta q_{sr,net} + q_{lr,net} \tag{2.100}$$

For three-dimensional calculations the source term $\hat{H}$ is given by

$$\hat{H} = \frac{\partial}{\partial z}\left(\frac{q_{sr,net}(1-\beta) e^{-\lambda(\eta - z)}}{\rho_0 c_p} \right) = \frac{q_{sr,net}(1-\beta) \dfrac{e^{-\lambda(\eta - z)}}{\lambda}}{\rho_0 c_p} \tag{2.101}$$

For two-dimensional calculations the source term $\hat{H}$ is given by

$$\hat{H} = \frac{q_v + q_c + q_{sr,net} + q_{lr,net}}{\rho_0 c_p} \tag{2.102}$$

The calculation of the latent heat flux, sensible heat flux, net short wave radiation, and net long wave radiation as described in the following sections.

In areas covered by ice the heat exchange is excluded.

2.10.1 Vaporisation

Dalton's law yields the following relationship for the vaporative heat loss (or latent flux), see Sahlberg, 1984

$$q_v = LC_e(a_1 + b_1 W_{2m})(Q_{water} - Q_{air}) \tag{2.103}$$

where $L = 2.5 \cdot 10^6 \ J/kg$ is the latent heat vaporisation (in the literature $L = 2.5 \cdot 10^6 - 2300\, T_{water}$ is commonly used); $C_e = 1.32 \cdot 10^{-3}$ is the moisture transfer coefficient (or Dalton number); W_{2m} is the wind speed 2 m above the sea surface; Q_{water} is the water vapour density close to the surface; Q_{air} is the water vapour density in the atmosphere; a_1 and b_1 are user specified constants. The default values are $a_1 = 0.5$ and $b_1 = 0.9$.

Measurements of Q_{water} and Q_{air} are not directly available but the vapour density can be related to the vapour pressure as

$$Q_i = \frac{0.2167}{T_i + T_k} e_i \tag{2.104}$$

in which subscript *i* refers to both water and air. The vapour pressure close to the sea, e_{water}, can be expressed in terms of the water temperature assuming that the air close to the surface is saturated and has the same temperature as the water

$$e_{water} = 6.11 e^K \left(\frac{1}{T_k} - \frac{1}{T_{water} + T_k} \right) \tag{2.105}$$

where $K = 5418\ °K$ and $T_K = 273.15\ °K$ is the temperature at 0 C. Similarly the vapour pressure of the air, e_{air}, can be expressed in terms of the air temperature and the relative humidity, R

$$e_{air} = R \cdot 6.11 e^K \left(\frac{1}{T_k} - \frac{1}{T_{air} + T_k} \right) \tag{2.106}$$

Replacing Q_{water} and Q_{air} with these expressions the latent heat can be written as

$$q_v = -P_v\left(a_1 + b_1 W_{2m}\right)\cdot \left(\frac{\exp\left(K\left(\frac{1}{T_k} - \frac{1}{T_{water}+T_k}\right)\right)}{T_{water}+T_k} - \frac{R\cdot\exp\left(K\left(\frac{1}{T_k} - \frac{1}{T_{air}+T_k}\right)\right)}{T_{air}+T_k} \right) \quad (2.107)$$

where all constants have been included in a new latent constant $P_v = 4370\ J\cdot°K/m^3$. During cooling of the surface the latent heat loss has a major effect with typical values up to 100 W/m^5.

2.10.2 Convection

The sensible heat flux, q_c (W/m^2), (or the heat flux due to convection) depends on the type of boundary layer between the sea surface and the atmosphere. Generally this boundary layer is turbulent implying the following relationship

$$q_c = \begin{cases} \rho_{air} c_{air} c_{heating} W_{10}(T_{air} - T_{water}) & T_{air} \geq T \\ \rho_{air} c_{air} c_{cooling} W_{10}(T_{air} - T_{water}) & T_{air} < T \end{cases} \quad (2.108)$$

where ρ_{air} is the air density 1.225 kg/m^6 $c_{air} = 1007\ J/(kg\cdot°K)$ is the specific heat of air; $c_{heating} = 0.0011$ and $c_{cooling} = 0.0011$, respectively, is the sensible transfer coefficient (or Stanton number) for heating and cooling (see Kantha and Clayson, 2000); W_{10} is the wind speed 10 m above the sea surface; T_{water} is the temperature at the sea surface; T_{air} is the temperature of the air.

The convective heat flux typically varies between 0 and 100 W/m^{5}1

2.10.3 Short wave radiation

Radiation from the sun consists of electromagnetic waves with wave lengths varying from 1,000 to 30,000 Å. Most of this is absorbed in the ozone layer, leaving only a fraction of the energy to reach the surface of the Earth. Furthermore, the spectrum changes when sunrays pass through the atmosphere. Most of the infrared and ultraviolet compound is absorbed such that the solar radiation on the Earth mainly consists of light with wave lengths between 4,000 and 9,000 Å. This radiation is normally termed short wave radiation. The intensity depends on the distance to the sun, declination angle and latitude,

extraterrestrial radiation and the cloudiness and amount of water vapour in the atmosphere (see Iqbal, 1983)

The eccentricity in the solar orbit, E_0, is given by

$$E_0 = \left(\frac{r_0}{r}\right)^2 = 1.000110 + 0.034221\cos(\Gamma) + 0.001280\sin(\Gamma) + 0.000719\cos(2\Gamma) + 0.000077\sin(2\Gamma) \quad (2.109)$$

where r_0 is the mean distance to the sun, r is the actual distance and the day angle $\Gamma\ (rad)$ is defined by

$$\Gamma = \frac{2\pi(d_n - 1)}{365} \quad (2.110)$$

and d_n is the Julian day of the year.

The daily rotation of the Earth around the polar axes contributes to changes in the solar radiation. The seasonal radiation is governed by the declination angle, $\delta\ (rad)$, which can be expressed by

$$\delta = 0.006918 - 0.399912\cos(\Gamma) + 0.07257\sin(\Gamma) - 0.006758\cos(2\Gamma) + 0.000907\sin(2\Gamma) - 0.002697\cos(3\Gamma) + 0.00148\sin(3\Gamma) \quad (2.111)$$

The day length, n_d, varies with δ. For a given latitude, ϕ, (positive on the northern hemisphere) the day length is given by

$$n_d = \frac{24}{\pi}\arccos\left(-\tan(\phi)\tan(\delta)\right) \quad (2.112)$$

and the sunrise angle, $\omega_{sr}\ (rad)$, and the sunset angle $\omega_{ss}\ (rad)$ are

$$\omega_{sr} = \arccos\left(-\tan(\phi)\tan(\delta)\right) \quad and \quad \omega_{ss} = \omega_{sr} \quad (2.113)$$

The intensity of short wave radiation on the surface parallel to the surface of the Earth changes with the angle of incidence. The highest intensity is in zenith and the lowest during sunrise and sunset. Integrated over one day the extraterrestrial intensity, $H_0\ (MJ/m^2/day)$, in short wave radiation on the surface can be derived as

$$H_0 = \frac{24}{\pi} q_{sc} E_0 \cos(\phi)\cos(\delta)\left(\sin(\omega_{sr}) - \omega_{sr}\cos(\omega_{sr})\right) \quad (2.114)$$

where $q_{sc} = 4.9212\ (MJ/m^2/h)$ is the solar constant.

For determination of daily radiation under cloudy skies, $H\ (MJ/m^2/day)$, the following relation is used

$$\frac{H}{H_0} = a_2 + b_2 \frac{n}{n_d} \tag{2.115}$$

in which n is the number of sunshine hours and n_d is the maximum number of sunshine hours. a_2 and b_2 are user specified constants. The default values are $a_2 = 0.295$ and $b_2 = 0.371$. The user-specified clearness coefficient corresponds to n/n_d. Thus the average hourly short wave radiation, $q_s\ (MJ/m^2/h)$, can be expressed as

$$q_s = \left(\frac{H}{H_0}\right) q_0 \left(a_3 + b_3 \cos(\omega_i)\right) \tag{2.116}$$

where

$$a_3 = 0.4090 + 0.5016 \sin\left(\omega_{sr} - \frac{\pi}{3}\right) \tag{2.117}$$

$$b_3 = 0.6609 + 0.4767 \sin\left(\omega_{sr} - \frac{\pi}{3}\right) \tag{2.118}$$

The extraterrestrial intensity, $q_0\ (MJ/m^2/h)$ and the hour angle ω_i is given by

$$q_0 = q_{sc} E_0 \left(\sin(\phi)\sin(\delta) + \frac{24}{\pi}\cos(\phi)\cos(\delta)\cos(\omega_i)\right) \tag{2.119}$$

$$\omega_i = \frac{\pi}{12}\left(12 + \Delta t_{displacement} + \frac{4}{60}(L_S - L_E) - \frac{E_t}{60} - t_{local}\right) \tag{2.120}$$

$\Delta t_{displacement}$ is the displacement hours due to summer time and the time meridian L_S is the standard longitude for the time zone. $\Delta t_{displacement}$ and L_S are user specified constants. The default values are $\Delta t_{displacement} = 0\ (h)$ and $L_S = 0$ (deg). L_E is the local longitude in degrees. $E_t\ (s)$ is the discrepancy in time due to solar orbit and is varying during the year. It is given by

$$E_t = \begin{pmatrix} 0.000075 + 0.001868\cos(\Gamma) - 0.032077\sin(\Gamma) \\ -0.014615\cos(2\Gamma) - 0.04089\sin(2\Gamma) \end{pmatrix} \cdot 229.18 \qquad (2.121)$$

Finally, t_{local} is the local time in hours.

Solar radiation that impinges on the sea surface does not all penetrate the water surface. Parts are reflected back and are lost unless they are backscattered from the surrounding atmosphere. This reflection of solar energy is termed the albedo. The amount of energy, which is lost due to albedo, depends on the angle of incidence and angle of refraction. For a smooth sea the reflection can be expressed as

$$\alpha = \frac{1}{2}\left(\frac{\sin^2(i-r)}{\sin^2(i+r)} + \frac{\tan^2(i-r)}{\tan^2(i+r)}\right) \qquad (2.122)$$

where *i* is the angle of incidence, *r* the refraction angle and α the reflection coefficient, which typically varies from 5 to 40 %. α can be approximated using

$$\alpha = \begin{cases} \dfrac{altitude}{5}\,0.48 & altitude < 5 \\ \dfrac{30 - altitude}{25}(0.48 - 0.05) & 5 \le altitude \le 30 \\ 0.05 & altitude > 30 \end{cases} \qquad (2.123)$$

where the altitude in degrees is given by

$$altitude = 90 - \left(\frac{180}{\pi}\arccos(\sin(\delta)\sin(\phi) + \cos(\delta)\cos(\phi)\cos(\omega_i))\right) \qquad (2.124)$$

Thus the net short wave radiation, $q_{s,net}$ (W/m^2), can eventually be expressed as

$$q_{sr,net} = (1-\alpha)q_s \frac{10^6}{3600} \qquad (2.125)$$

2.10.4 Long wave radiation

A body or a surface emits electromagnetic energy at all wavelengths of the spectrum. The long wave radiation consists of waves with wavelengths between 9,000 and 25,000 Å. The radiation in this interval is termed infrared radiation and is emitted from the

atmosphere and the sea surface. The long wave emittance from the surface to the atmosphere minus the long wave radiation from the atmosphere to the sea surface is called the net long wave radiation and is dependent on the cloudiness, the air temperature, the vapour pressure in the air and the relative humidity. The net outgoing long wave radiation, $q_{lr,net}\ (W/m^2)$, is given by Brunt's equation (See Lind and Falkenmark, 1972)

$$q_{lr,net} = -\sigma_{sb}\left(T_{air} + T_K\right)^4\left(a - b\sqrt{e_d}\right)\left(c + d\frac{n}{n_d}\right) \qquad (2.126)$$

where e_d is the vapour pressure at dew point temperature measured in *mb*; n is the number of sunshine hours, n_d is the maximum number of sunshine hours; $\sigma_{sb} = 5.6697 \cdot 10^{-8}\ W/(m^2 \cdot °K^4)$ is Stefan Boltzman's constant; $T_{air}\,(°C)$ is the air temperature. The coefficients *a*, *b*, *c* and *d* are given as

$$a = 0.56; b = 0.077 mb^{-½}; c = 0.10; d = .90 \qquad (2.127)$$

The vapour pressure is determined as

$$e_d = 10 \cdot R\ e_{saturated} \qquad (2.128)$$

where *R* is the relative humidity and the saturated vapour pressure, $e_{saturated}\ (kPa)$, with 100 % relative humidity in the interval from –51 to 52 °C can be estimated by

$$e_{saturated} = 3.38639 \cdot \left(\left(7.38 \cdot 10^{-3} \cdot T_{air} + 0.8072\right)^8 - 1.9 \cdot 10^{-5}\left|1.8 \cdot T_{air} + 48\right| + 1.316 \cdot 10^{-3}\right) \qquad (2.129)$$

3 NUMERICAL SOLUTION

3.1 Spatial Discretization

The discretization in solution domain is performed using a finite volume method. The spatial domain is discretized by subdivision of the continuum into non-overlapping cells/elements.

In the two-dimensional case the elements can be arbitrarily shaped polygons, however, here only triangles and quadrilateral elements are considered.

In the three-dimensional case a layered mesh is used: in the horizontal domain an unstructured mesh is used while in the vertical domain a structured mesh is used (see Figure 3.1gure 3.1). The vertical mesh is based on either sigma coordinates or combined sigma/z-level coordinates. For the hybrid sigma/z-level mesh sigma coordinates are used from the free surface to a specified depth and z-level coordinates are used below. The different types of vertical mesh are illustrated in Figure 3.2. The elements in the sigma domain and the z-level domain can be prisms with either a 3-sided or 4-sided polygonal base. Hence, the horizontal faces are either triangles or quadrilateral element. The elements are perfectly vertical and all layers have identical topology.

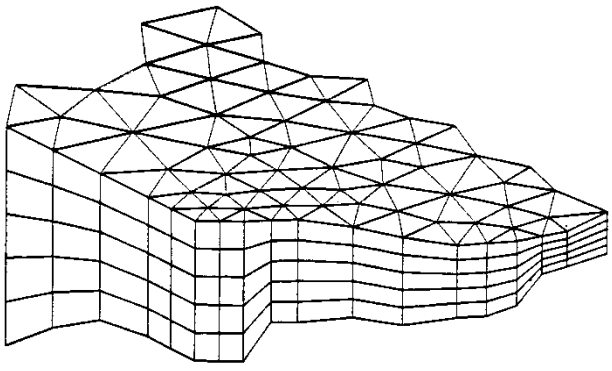

Figure 3.1 Principle of meshing for the three-dimensional case

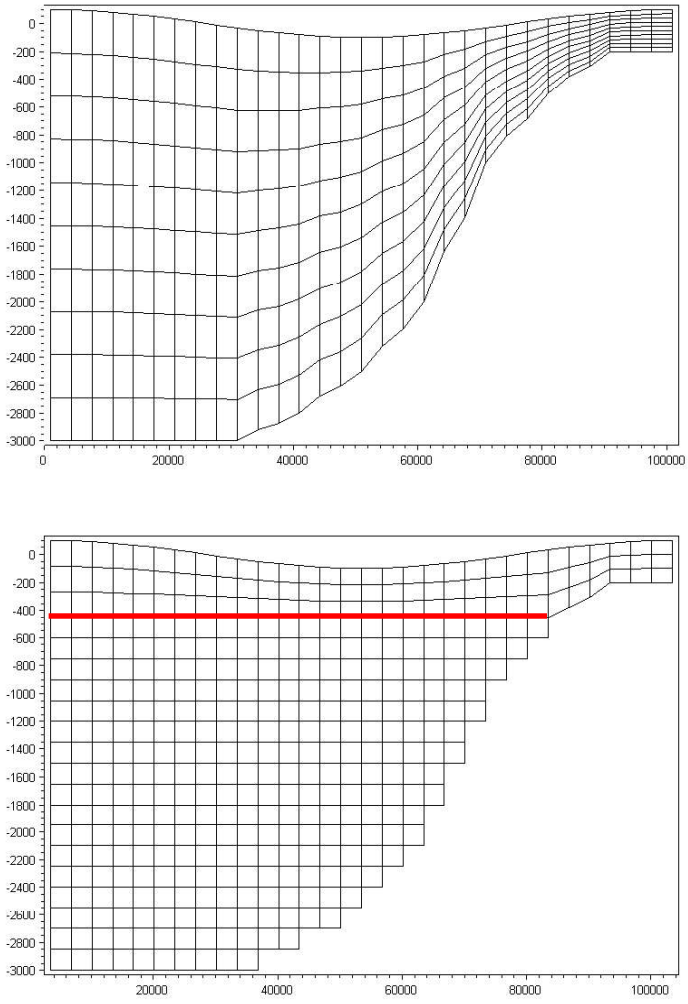

Figure 3.2 *Illustrations of the different vertical grids. Upper: sigma mesh, Lower: combined sigma/z-level mesh with simple bathymetry adjustment. The red line shows the interface between the z-level domain and the sigma-level domain*

The most important advantage using sigma coordinates is their ability to accurately represent the bathymetry and provide consistent resolution near the bed. However, sigma coordinates can suffer from significant errors in the horizontal pressure gradients, advection and mixing terms in areas with sharp topographic changes (steep slopes). These errors can give rise to unrealistic flows.

The use of z-level coordinates allows a simple calculation of the horizontal pressure gradients, advection and mixing terms, but the disadvantages are their inaccuracy in representing the bathymetry and that the stair-step representation of the bathymetry can result in unrealistic flow velocities near the bottom.

3.1.1 Vertical Mesh

For the vertical discretization both a standard sigma mesh and a combined sigma/z-level mesh can be used. For the hybrid sigma/z-level mesh sigma coordinates are used from the free surface to a specified depth, z_σ, and z-level coordinates are used below. At least one sigma layer is needed to allow changes in the surface elevation.

Sigma

In the sigma domain a constant number of layers, N_σ, are used and each sigma layer is a fixed fraction of the total depth of the sigma layer, h_σ, where h_σ = $\eta - z_b$ or z_σ. The discretization in the sigma domain is given by a number of discrete σ-levels $\{\sigma_i, i = 0, N_\sigma + 1\}$. Here σ varies from $\sigma_1 = 0$ at the bottom interface of the lowest sigma layer to $\sigma_{N_\sigma + 1} = 1$ at the free surface.

Variable sigma coordinates can be obtained using a discrete formulation of the general vertical coordinate (s-coordinate) system proposed by Song and Haidvogel (1994). First an equidistant discretization in a s-coordinate system *(-1≤ s ≤0)* is defined

$$s_i = -\frac{N_\sigma + 1 - i}{N_\sigma} \qquad i = 0, N_\sigma + 1 \tag{3.1}$$

The discrete sigma coordinates can then be determined by

$$\sigma_i = 1 + \sigma_c s_i + (1 - \sigma_c) c(s_i) \quad i = 1, (N_\sigma + 1) \tag{3.2}$$

where

$$c(s) = (1 - b)\frac{\sinh(\theta s)}{\sinh(\theta)} + b\frac{\tanh\left(\theta\left(s + \frac{1}{2}\right)\right) - \tanh\frac{\theta}{2}}{2\tanh\frac{\theta}{2}} \tag{3.3}$$

Here σ_c is a weighting factor between the equidistant distribution and the stretch distribution, θ is the surface control parameter and b is the bottom control parameter. The range for the weighting factor is $0<\sigma_c\leq 1$ where the value 1 corresponds to equidistant distribution and 0 corresponds to stretched distribution. A small value of σ_c can result in linear instability. The range of the surface control parameter is $0<\theta\leq 20$ and the range of the bottom control parameter is $0\leq b\leq 1$. If $\theta<<1$ and $b=0$ an equidistant vertical resolution is obtained. By increasing the value of the θ, the highest resolution is achieved near the surface. If $\theta>0$ and $b=1$ a high resolution is obtained both near the surface and near the bottom.

Examples of a mesh using variable vertical discretization are shown in Figure 3.3 and Figure 3.4.

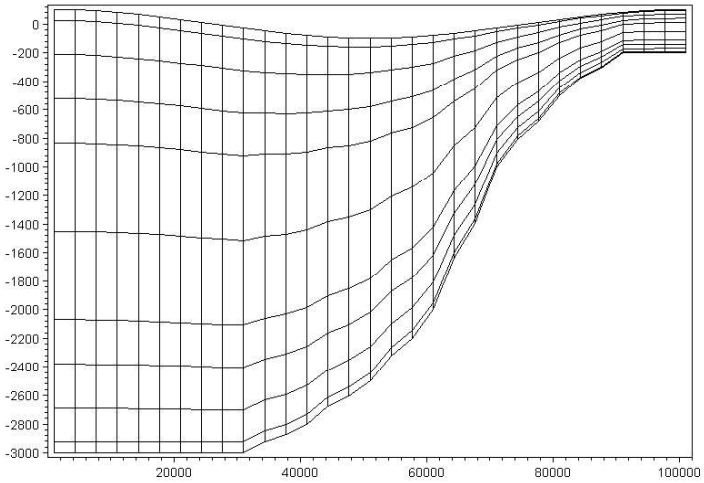

Figure 3.3 Example of vertical distribution using layer thickness distribution. Number of layers: 10, thickness of layers 1 to 10: .025, 0.075, 0.1, 0.01, 0.02, 0.02, 0.1, 0.1, 0.075, 0.025

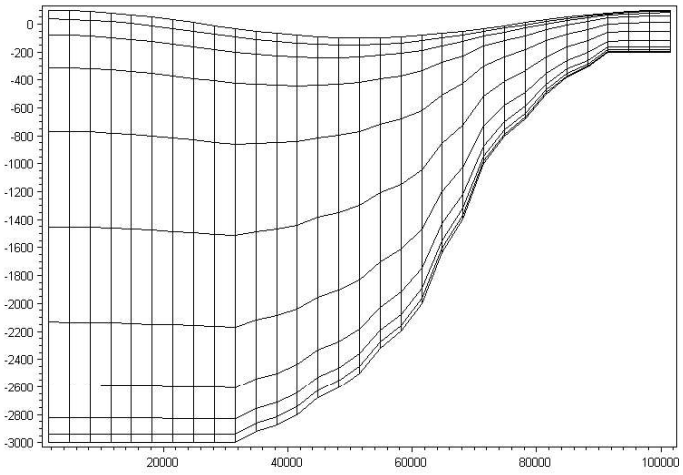

Figure 3.4 Example of vertical distribution using variable distribution. Number of layers: 10, σ_c = 0.1, θ = 5, b = 1

Combined sigma/z-level

In the z-level domain the discretization is given by a number of discrete z-levels $\{z_i\}_{i=50,N_z/5}$ where N_z is the number of layers in the z-level domain. z_1 is the minimum z-level and $z_{N_z/5}$ is the maximum z-level, which is equal to the sigma depth, z_σ. The corresponding layer thickness is given by

$$\Delta z_i = z_{i/5} - z_i \qquad i = 50 N_z \tag{3.4}$$

The discretization is illustrated in Figure 3.5 and Figure 3.6.

Using standard z-level discretization the bottom depth is rounded to the nearest z-level. Hence, for a cell in the horizontal mesh with the cell-averaged depth, z_b, the cells in the corresponding column in the z-domain are included if the following criteria is satisfied

$$(z_{k+1/2} - z_k) \geq z_b \quad k = 1, N_z \tag{3.5}$$

The cell-averaged depth, z_b, is calculated as the mean value of the depth at the vortices of each cell. For the standard z-level discretization the minimum depth is given by z_1. Too take into account the correct depth for the case where the bottom depth is below the minimum z-level ($z_1 < z_b$) a bottom fitted approach is used. Here, a correction factor, f_1, for the layer thickness in the bottom cell is introduced. The correction factor is used in the calculation of the volume and face integrals. The correction factor for the bottom cell is calculated by

$$f_1 = \frac{(z_2 - z_b)}{\Delta z_1} \tag{3.6}$$

The corrected layer thickness is given by $\Delta z_1^* = f_1 \Delta z_1$. The simple bathymetry adjustment approach is illustrated in Figure 3.5.

For a more accurate representation of the bottom depth an advanced bathymetry adjustment approach can be used. For a cell in the horizontal mesh with the cell-averaged depth, z_b, the cells in the corresponding column in the z-domain are included if the following criteria is satisfied

$$z_{k+1/2} > z_b \qquad k = 1, N_z \tag{3.7}$$

A correction factor, f_i, is introduced for the layer thickness

$$f_i = max\left(\frac{(z_{i+1/2} - z_b)}{\Delta z_i}, \frac{z_{min}}{\Delta z_i}\right) \qquad z_i \leq z_b \leq z_{i+1/2} \text{ or } z_1 \tag{3.8}$$

$$f_i = 1 \qquad z_1 \geq z_b$$

A minimum layer thickness, Δz_{min}, is introduced to avoid very small values of the correction factor. The correction factor is used in the calculation of the volume and face integrals. The corrected layer thicknesses are given by $\{\Delta z_i^* = f_i \Delta z_i, i = 1, N_z\}$. The advanced bathymetry adjustment approach is illustrated in Figure 3.6.

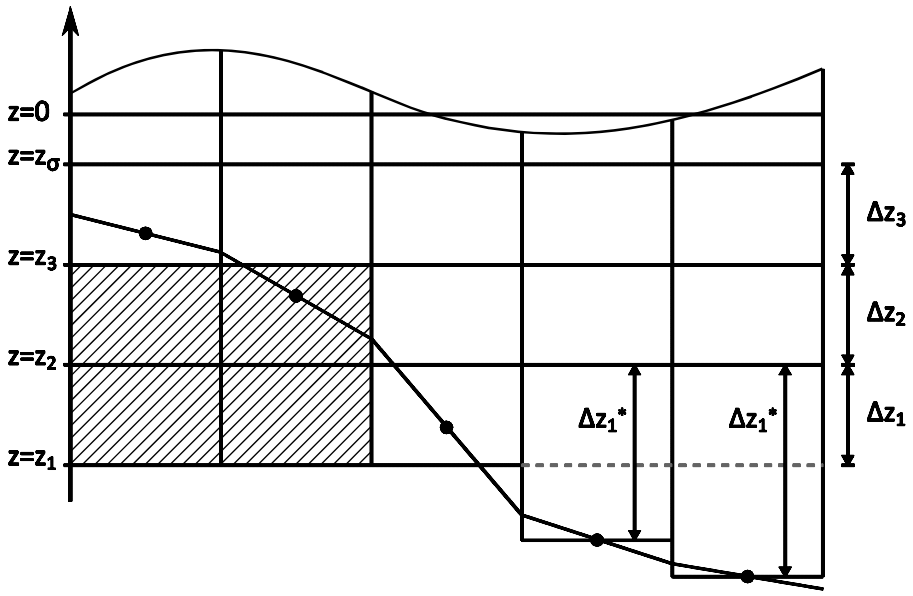

Figure 3.5 Simple bathymetry adjustment approach

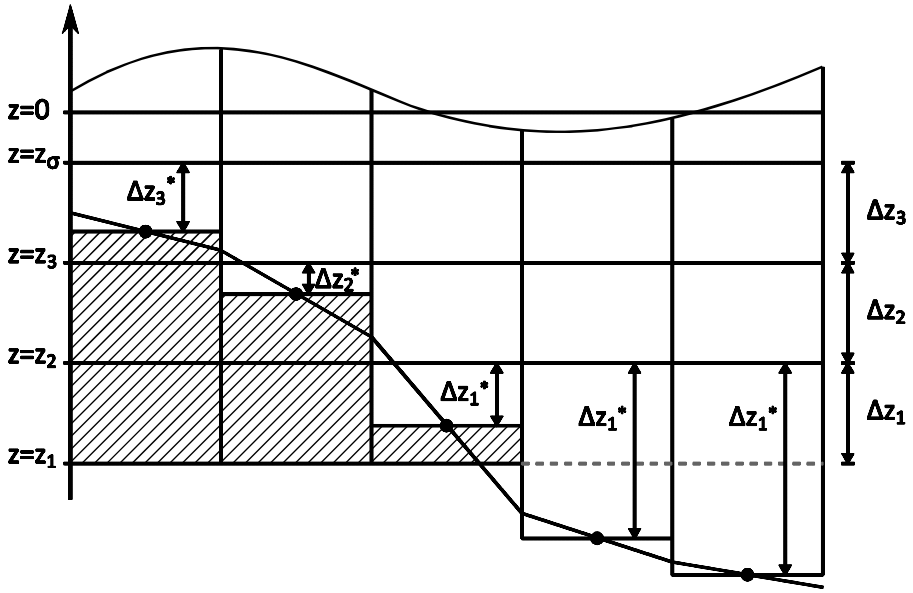

Figure 3.6 Advanced bathymetry adjustment approach

3.1.2 Shallow water equations

The integral form of the system of shallow water equations can in general form be written

$$\frac{\partial \boldsymbol{U}}{\partial t} + \nabla \cdot \boldsymbol{F}(\boldsymbol{U}) = \boldsymbol{S}(\boldsymbol{U}) \tag{3.9}$$

where $\boldsymbol{U}$ is the vector of conserved variables, $\boldsymbol{F}$ is the flux vector function and $\boldsymbol{S}$ is the vector of source terms.

In Cartesian co-ordinates the system of 2D shallow water equations can be written

$$\frac{\partial \boldsymbol{U}}{\partial t}+\frac{\partial\left(\boldsymbol{F}_x^I-\boldsymbol{F}_x^V\right)}{\partial x}+\frac{\partial\left(\boldsymbol{F}_y^I-\boldsymbol{F}_y^V\right)}{\partial y}=\boldsymbol{S} \tag{3.10}$$

where the superscripts *I* and *V* denote the inviscid (convective) and viscous fluxes, respectively and where

$$\boldsymbol{U}=\begin{bmatrix} h \\ h\bar{u} \\ h\bar{v} \end{bmatrix},$$

$$\boldsymbol{F}_x^{\,I}=\begin{bmatrix} h\bar{u} \\ h\bar{u}^2+\frac{1}{2}g(h^2-d^2) \\ h\bar{u}\bar{v} \end{bmatrix}, \quad \mathrm{F}_x^{\,V}=\begin{bmatrix} 0 \\ hA\left(2\frac{\partial \bar{u}}{\partial x}\right) \\ hA\left(\frac{\partial \bar{u}}{\partial y}+\frac{\partial \bar{v}}{\partial x}\right) \end{bmatrix}$$

$$\boldsymbol{F}_y^{\,I}=\begin{bmatrix} h\bar{v} \\ h\bar{v}\bar{u} \\ h\bar{v}^2+\frac{1}{2}g(h^2-d^2) \end{bmatrix}_a, \quad \mathrm{F}_y^{\,V}=\begin{bmatrix} 0 \\ hA\left(\frac{\partial \bar{u}}{\partial y}+\frac{\partial \bar{v}}{\partial x}\right) \\ hA\left(2\frac{\partial \bar{v}}{\partial x}\right) \end{bmatrix} \tag{3.11}$$

$$\boldsymbol{S}=\begin{bmatrix} 0 \\ g\eta\frac{\partial d}{\partial x}+f\bar{v}h-\frac{h}{\rho_0}\frac{\partial p_a}{\partial x}-\frac{gh^2}{2\rho_0}\frac{\partial \rho}{\partial x}-\frac{1}{\rho_0}\left(\frac{\partial s_{xx}}{\partial x}+\frac{\partial s_{xy}}{\partial y}\right) \\ \qquad +\frac{\tau_{sx}}{\rho_0}-\frac{\tau_{bx}}{\rho_0}+hu_s \\ g\eta\frac{\partial d}{\partial y}-f\bar{u}h-\frac{h}{\rho_0}\frac{\partial p_a}{\partial y}-\frac{gh^2}{2\rho_0}\frac{\partial \rho}{\partial y}-\frac{1}{\rho_0}\left(\frac{\partial s_{yx}}{\partial x}+\frac{\partial s_{yy}}{\partial y}\right) \\ \qquad +\frac{\tau_{sy}}{\rho_0}-\frac{\tau_{by}}{\rho_0}+hv_s \end{bmatrix}$$

In Cartesian co-ordinates the system of 3D shallow water equations can be written

$$\frac{\partial \boldsymbol{U}}{\partial t}+\frac{\partial \boldsymbol{F}_x^I}{\partial x'}+\frac{\partial \boldsymbol{F}_y^I}{\partial y'}+\frac{\partial \boldsymbol{F}_\sigma^I}{\partial \sigma}+\frac{\partial \boldsymbol{F}_x^V}{\partial x}+\frac{\partial \boldsymbol{F}_y^V}{\partial y}+\frac{\partial \boldsymbol{F}_\sigma^V}{\partial \sigma}=\boldsymbol{S} \tag{3.12}$$

where the superscripts *I* and *V* denote the inviscid (convective) and viscous fluxes, respectively and where

$$\boldsymbol{U}=\begin{bmatrix} h \\ hu \\ hv \end{bmatrix},$$

$$\boldsymbol{F}_x^{\,I}=\begin{bmatrix} h\bar{u} \\ hu^2+\frac{1}{2}g(h^2-d^2) \\ huv \end{bmatrix},\quad \boldsymbol{F}_x^{\,V}=\begin{bmatrix} 0 \\ hA\left(2\frac{\partial u}{\partial x}\right) \\ hA\left(\frac{\partial u}{\partial y}+\frac{\partial v}{\partial x}\right) \end{bmatrix}$$

$$\boldsymbol{F}_y^{\,I}=\begin{bmatrix} h\bar{v} \\ hvu \\ hv^2+\frac{1}{2}g(h^2-d^2) \end{bmatrix},\quad \boldsymbol{F}_y^{\,V}=\begin{bmatrix} 0 \\ hA\left(\frac{\partial u}{\partial y}+\frac{\partial v}{\partial x}\right) \\ hA\left(2\frac{\partial v}{\partial x}\right) \end{bmatrix} \tag{3.13}$$

$$\boldsymbol{F}_\sigma^{\,I}=\begin{bmatrix} h\omega \\ h\omega u \\ h\omega v \end{bmatrix},\quad \boldsymbol{F}_\sigma^{\,V}=\begin{bmatrix} 0 \\ \frac{\upsilon_t}{h}\frac{\partial u}{\partial \sigma} \\ \frac{\upsilon_t}{h}\frac{\partial v}{\partial \sigma} \end{bmatrix}$$

$$\boldsymbol{S}=\begin{bmatrix} 0 \\ g\eta\frac{\partial d}{\partial x}+fvh-\frac{h}{\rho_0}\frac{\partial p_a}{\partial x'}-\frac{hg}{\rho_0}\int_z^\eta\frac{\partial \rho}{\partial x}dz-\frac{1}{\rho_0}\left(\frac{\partial s_{xx}}{\partial x}+\frac{\partial s_{xy}}{\partial y}\right) \\ g\eta\frac{\partial d}{\partial y}-fuh-\frac{h}{\rho_0}\frac{\partial p_a}{\partial y'}-\frac{hg}{\rho_0}\int_z^\eta\frac{\partial \rho}{\partial y}dz-\frac{1}{\rho_0}\left(\frac{\partial s_{yx}}{\partial x}+\frac{\partial s_{yy}}{\partial y}\right) \end{bmatrix}$$

Integrating Eq. (3.9) over the *i*th cell and using Gauss's theorem to rewrite the flux integral gives

$$\int_{A_i}\frac{\partial \boldsymbol{U}}{\partial t}d\Omega+\int_{\Gamma_i}(\boldsymbol{F}\cdot\boldsymbol{n})\,ds=\int_{A_i}\boldsymbol{S}(\boldsymbol{U})d\Omega \tag{3.14}$$

where A_i is the area/volume of the cell Ω is the integration variable defined on A_i, Γ_i is the boundary of the *i*th cell and *ds* is the integration variable along the boundary. ***n*** is the unit outward normal vector along the boundary. Evaluating the area/volume integrals by a one-point quadrature rule, the quadrature point being the centroid of the cell, and evaluating the boundary intergral using a mid-point quadrature rule, Eq. (3.14) can be written

$$\frac{\partial U_i}{\partial t} + \frac{1}{A_i}\sum_{j}^{NS} \boldsymbol{F}\cdot\boldsymbol{n}\,\Delta\Gamma_j = S_i \qquad (3.15)$$

Here U_i and S_i, respectively, are average values of U and S over the *i*th cell and stored at the cell centre, NS is the number of sides of the cell, n_j is the unit outward normal vector at the *j*th side and $\Delta\Gamma_j$ the length/area of the *j*th interface.

Both a first order and a second order scheme can be applied for the spatial discretization.

For the 2D case an approximate Riemann solver (Roe's scheme, see Roe, 1981) is used to calculate the convective fluxes at the interface of the cells. Using the Roe's scheme the dependent variables to the left and to the right of an interface have to be estimated. Second-order spatial accuracy is achieved by employing a linear gradient-reconstruction technique. The average gradients are estimated using the approach by Jawahar and Kamath, 2000. To avoid numerical oscillations a second order TVD slope limiter (Van Leer limiter, see Hirch, 1990 and Darwish, 2003) is used.

For the 3D case an approximate Riemann solver (Roe's scheme, see Roe, 1981) is used to calculate the convective fluxes at the vertical interface of the cells (x'y'-plane). Using the Roe's scheme the dependent variables to the left and to the right of an interface have to be estimated. Second-order spatial accuracy is achieved by employing a linear gradient-reconstruction technique. The average gradients are estimated using the approach by Jawahar and Kamath, 2000. To avoid numerical oscillations a second order TVD slope limiter (Van Leer limiter, see Hirch, 1990 and Darwish, 2003) is used. The convective fluxes at the horizontal interfaces (vertical line) are derived using first order upwinding for the low order scheme. For the higher order scheme the fluxes are approximated by the mean value of the fluxes calculated based on the cell values above and below the interface for the higher order scheme.

3.1.3 Transport equations

The transport equations arise in the salt and temperature model, the turbulence model and the generic transport model. They all share the form of Equation Eq. (2.20) in Cartesian coordinates. For the 2D case the integral form of the transport equation can be given by Eq. (3.9) where

$$\boldsymbol{U} = h\bar{C}$$

$$\begin{aligned} \boldsymbol{F}^I &= \left[h\bar{u}\bar{C}, \quad h\bar{v}\bar{C} \right] \\ \boldsymbol{F}^V &= \left[hD_h \frac{\partial \bar{C}}{\partial x}, \quad hD_h \frac{\partial \bar{C}}{\partial y} \right] \end{aligned} \tag{3.16}$$

$$\boldsymbol{S} = -hk_p\bar{C} + hC_sS.$$

For the 3D case the integral form of the transport equation can be given by Eq. (3.9) where

$$\boldsymbol{U} = hC$$

$$\begin{aligned} \boldsymbol{F}^I &= \left[huC, \quad hvC, \quad h\omega C \right] \\ \boldsymbol{F}^V &= \left[hD_h\partial \frac{\partial C}{\partial x}, \quad hD_h\partial \frac{\partial C}{\partial y}, \quad h\frac{D_h}{h}\partial \frac{\partial C}{\partial \sigma} \right] \end{aligned} \tag{3.17}$$

$$\boldsymbol{S} = -hk_pC + hC_sS.$$

The discrete finite volume form of the transport equation is given by Eq. (3.15). As for the shallow water equations both a first order and a second order scheme can be applied for the spatial discretization.

In 2D the low order approximation uses simple first order upwinding, i.e., element average values in the upwinding direction are used as values at the boundaries. The higher order version approximates gradients to obtain second order accurate values at the boundaries. Values in the upwinding direction are used. To provide stability and minimize oscillatory effects, a TVD-MUSCL limiter is applied (see Hirch, 1990, and Darwish, 2003).

In 3D the low order version uses simple first order upwinding. The higher order version approximates horizontal gradients to obtain second order accurate values at the horizontal boundaries. Values in the upwinding direction are used. To provide stability and minimize oscillatory effects, an ENO (Essentially Non-Oscillatory) type

procedure is applied to limit the horizontal gradients. In the vertical direction a 3rd order ENO procedure is used to obtain the vertical face values (Shu, 1997).

3.2 Time Integration

Consider the general form of the equations

$$\frac{\partial \boldsymbol{U}}{\partial t} = \boldsymbol{G}(\boldsymbol{U}) \tag{3.18}$$

For 2D simulations, there are two methods of time integration for both the shallow water equations and the transport equations: A low order method and a higher order method. The low order method is a first order explicit Euler method

$$\boldsymbol{U}_{n+1} = \boldsymbol{U}_n + \Delta t\ \boldsymbol{G}(\boldsymbol{U}_n) \tag{3.19}$$

where Δt is the time step interval. The higher order method uses a second order Runge Kutta method on the form:

$$\begin{aligned} \boldsymbol{U}_{n+\frac{1}{2}} &= \boldsymbol{U}_n + \tfrac{1}{2}\Delta t\ \boldsymbol{G}(\boldsymbol{U}_n) \\ \boldsymbol{U}_{n+1} &= \boldsymbol{U}_n + \Delta t\ \boldsymbol{G}(\boldsymbol{U}_{n+\frac{1}{2}}) \end{aligned} \tag{3.20}$$

For 3D simulations the time integration is semi-implicit. The horizontal terms are treated implicitly and the vertical terms are treated implicitly or partly explicitly and partly implicitly. Consider the equations in the general semi-implicit form.

$$\frac{\partial \boldsymbol{U}}{\partial t} = \boldsymbol{G}_h(\boldsymbol{U}) + \boldsymbol{G}_v(B\boldsymbol{U}) = \boldsymbol{G}_h(\boldsymbol{U}) + \boldsymbol{G}_v^I(\boldsymbol{U}) + \boldsymbol{G}_v^V(\boldsymbol{U}) \tag{3.21}$$

where the h and v subscripts refer to horizontal and vertical terms, respectively, and the superscripts refer to invicid and viscous terms, respectively. As for 2D simulations, there is a lower order and a higher order time integration method.

The low order method used for the 3D shallow water equations can written as

$$\boldsymbol{U}_{n+1} - \tfrac{1}{2}\Delta t\left(\boldsymbol{G}_v(\boldsymbol{U}_{n+1}) + \boldsymbol{G}_v(\boldsymbol{U}_n)\right) = \boldsymbol{U}_n + \Delta t\ \boldsymbol{G}_h(\boldsymbol{U}_n) \tag{3.22}$$

The horizontal terms are integrated using a first order explicit Euler method and the vertical terms using a second order implicit trapezoidal rule. The higher order method can be written

$$\begin{aligned} \boldsymbol{U}_{n+1/2} - \tfrac{1}{4}\Delta t \ \left(\boldsymbol{G}_v(\boldsymbol{U}_{n+1/2}) + \boldsymbol{G}_v(\boldsymbol{U}_n)\right) &= \boldsymbol{U}_n + \tfrac{1}{2}\Delta t \ \boldsymbol{G}_h(\boldsymbol{U}_n) \\ \boldsymbol{U}_{n+1} - \tfrac{1}{2}\Delta t \ \left(\boldsymbol{G}_v(\boldsymbol{U}_{n+1}) + \boldsymbol{G}_v(\boldsymbol{U}_n)\right) &= \boldsymbol{U}_n + \Delta t \ \boldsymbol{G}_h(\boldsymbol{U}_{n+1/2}) \end{aligned} \tag{3.23}$$

The horizontal terms are integrated using a second order Runge Kutta method and the vertical terms using a second order implicit trapezoidal rule.

The low order method used for the 3D transport equation can written as

$$\boldsymbol{U}_{n+1} - \tfrac{1}{2}\Delta t\left(\ \boldsymbol{G}_v^V(\boldsymbol{U}_{n+1}) + \boldsymbol{G}_v^V(\boldsymbol{U}_n)\right) = \boldsymbol{U}_n + \Delta t \ \boldsymbol{G}_h(\boldsymbol{U}_n) + \Delta t \ \boldsymbol{G}_v^I(\tag{3.24}$$

The horizontal terms and the vertical convective terms are integrated using a first order explicit Euler method and the vertical viscous terms are integrated using a second order implicit trapezoidal rule. The higher order method can be written

$$\begin{aligned} \boldsymbol{U}_{n+1/2} - \tfrac{1}{4}\Delta t \ \left(\boldsymbol{G}_v^V(\boldsymbol{U}_{n+1/2}) + \boldsymbol{G}_v^V(\boldsymbol{U}_n)\right) = \\ \boldsymbol{U}_n + \tfrac{1}{2}\Delta t \ \boldsymbol{G}_h(\boldsymbol{U}_n) + \tfrac{1}{2}\Delta t \ \boldsymbol{G}_v^I(\boldsymbol{U}_n) \\ \boldsymbol{U}_{n+1} - \tfrac{1}{2}\Delta t \ \left(\boldsymbol{G}_v^V(\boldsymbol{U}_{n+1}) + \boldsymbol{G}_v^V(\boldsymbol{U}_n)\right) = \\ \boldsymbol{U}_n + \Delta t \ \boldsymbol{G}_h(\boldsymbol{U}_{n+1/2}) + \Delta t \ \boldsymbol{G}_v^I(\boldsymbol{U}_{n+1/2}) \end{aligned} \tag{3.25}$$

The horizontal terms and the vertical convective terms are integrated using a second order Runge Kutta method and the vertical terms are integrated using a second order implicit trapezoidal rule for the vertical terms.

3.3 Boundary Conditions

3.3.1 Closed boundaries

Along closed boundaries (land boundaries) normal fluxes are forced to zero for all variables. For the momentum equations this leads to full-slip along land boundaries.

3.3.2 Open boundaries

The open boundary conditions can be specified either in form of a unit discharge or as the surface elevation for the hydrodynamic equations. For transport equations either a specified value or a specified gradient can be given.

3.3.3 Flooding and drying

The approach for treatment of the moving boundaries problem (flooding and drying fronts) is based on the work by Zhao et al. (1994) and Sleigh et al. (1998). When the depths are small the problem is reformulated and only when the depths are very small the elements/cells are removed from the calculation. The reformulation is made by setting the momentum fluxes to zero and only taking the mass fluxes into consideration.

The depth in each element/cell is monitored and the elements are classified as dry, partially dry or wet. Also the element faces are monitored to identify flooded boundaries.

- An element face is defined as flooded if the following two criteria are satisfied: Firstly, the water depth at one side of face must be less than a tolerance depth, h_{dry}, and the water depth at the other side of the face larger than a tolerance depth, h_{flood}. Secondly, the sum of the still water depth at the side for which the water depth is less than h_{dry} and the surface elevation at the other side must be larger than zero.

- An element is dry if the water depth is less than a tolerance depth, h_{dry}, and no of the element faces are flooded boundaries. The element is removed from the calculation.

- An element is partially dry if the water depth is larger than h_{dry} and less than a tolerance depth, h_{wet}, or when the depth is less than the h_{dry} and one of the element faces is a flooded boundary. The momentum fluxes are set to zero and only the mass fluxes are calculated.

- An element is wet if the water depth is greater than h_{wet}. Both the mass fluxes and the momentum fluxes are calculated.

The wetting depth, h_{wet}, must be larger than the drying depth, h_{dry}, and flooding depth, h_{flood}, must satisfy

$$h_{dry} < h_{flood} < h_{wet} \tag{3.26}$$

The default values are $h_{dry} = 0.005\,m$, $h_{flood} = 0.05\,m$ and $h_{wet} = 0.1\,m$.

Note, that for very small values of the tolerance depth, h_{wet}, unrealistically high flow velocities can occur in the simulation and give cause to stability problems.

4 VALIDATION

The new finite-volume model has been successfully tested in a number of basic, idealised situations for which computed results can be compared with analytical solutions or information from the literature. The model has also been applied and tested in more natural geophysical conditions; ocean scale, inner shelves, estuaries, lakes and overland, which are more realistic and complicated than academic and laboratory tests. A detailed validation report is under preparation.

This chapter presents a comparison between numerical model results and laboratory measurements for a dam-break flow in an L-shaped channel.

Additional information on model validation and applications can be found here

http://mikebydhi.com/Download/DocumentsAndTools/PapersAndDocs.aspx

4.1 Dam-break Flow through Sharp Bend

The physical model to be studied combines a square-shaped upstream reservoir and an L-shaped channel. The flow will be essentially two-dimensional in the reservoir and at the angle between the two reaches of the L-shaped channel. However, there are numerical and experimental evidences that the flow will be mostly unidimensional in both rectilinear reaches. Two characteristics or the dam-break flow are of special interest, namely

- The "damping effect" of the corner
- The upstream-moving hydraulic jump which forms at the corner

The multiple reflections of the expansion wave in the reservoir will also offer an opportunity to test the 2D capabilities of the numerical models. As the flow in the reservoir will remain subcritical with relatively small-amplitude waves, computations could be checked for excessive numerical dissipation.

4.1.1 Physical experiments

A comprehensive experimental study of a dam-break flow in a channel with a 90 bend has been reported by Frazão and Zech (2002, 1999a, 1999b). The channel is made of a 3.92 and a 2.92 metre long and 0.495 metre wide rectilinear reaches connected at right angle by a 0.495 x 0.495 m square element. The channel slope is equal to zero. A guillotine-type gate connects this L-shaped channel to a 2.44 x 2.39 m

(nearly) square reservoir. The reservoir bottom level is 33 cm lower that the channel bed level. At the downstream boundary a chute is placed. See the enclosed figure for details.

Frazão and Zech performed measurements for both dry bed and wet bed condition. Here comparisons are made for the case where the water in the reservoir is initially at rest, with the free surface 20 cm above the channel bed level, i.e. the water depth in the reservoir is 53 cm. The channel bed is initially dry. The Manning coefficients evaluated through steady-state flow experimentation are 0.0095 and 0.0195 $s/m^{1/3}$, respectively, for the bed and the walls of the channel.

The water level was measured at six gauging points. The locations of the gauges are shown in Figure 4.1 and the co-ordinates are listed in Table 4.1.

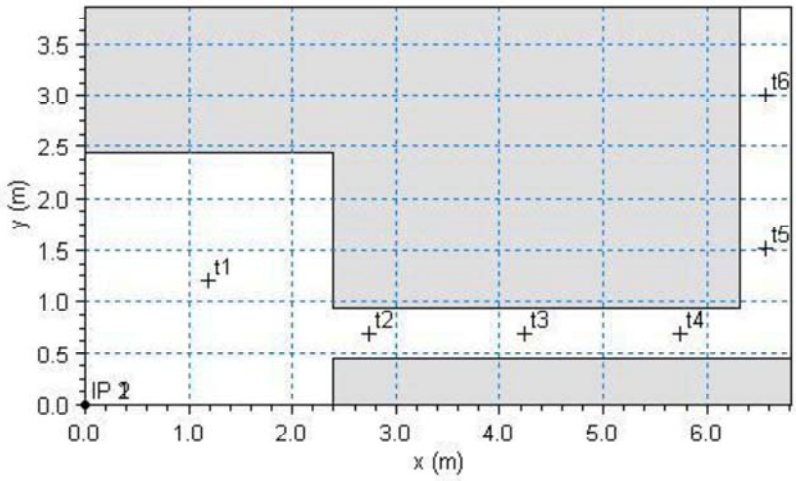

Figure 4.1 Set-up of the experiment by Frazão and Zech (2002)

Table 4.1 Location of the gauging points

Location	x (m)	y (m)
T1	1.19	1.20
T2	2.74	0.69
T3	4.24	0.69
T4	5.74	0.69
T5	6.56	1.51
T6	6.56	3.01

4.1.2 Numerical experiments

Simulations are performed using both the two-dimensional and the three-dimensional shallow water equations.

An unstructured mesh is used containing 18311 triangular elements and 9537 nodes. The minimum edge length is 0.01906 m and the maximum edge length is 0.06125 m. In the 3D simulation 10 layers is used for the vertical discretization. The time step is 0.002 s. At the downstream boundary, a free outfall (absorbing) boundary condition is applied. The wetting depth, flooding depth and drying depth are 0.002 m, 0.001 m and 0.0001 m, respectively.

A constant Manning coefficient of 105.26 $m^{1/3}/s$ is applied in the 2D simulations, while a constant roughness height of $5 \cdot 10^{-08}$ m is applied in the 3D simulation.

4.1.3 Results

In Figure 4.2 time series of calculated surface elevations at the six gauges locations are compared to the measurements. In Figure 4.3 contour plots of the surface elevations are shown at T = 1.6, 3.2 and 4.8 s (two-dimensional simulation).

In Figure 4.4 a vector plot and contour plots of the current speed at a vertical profile along the centre line (from (x,y)=(5.7, 0.69) to (x,y)=(6.4, 0.69)) at T = 6.4 s is shown.

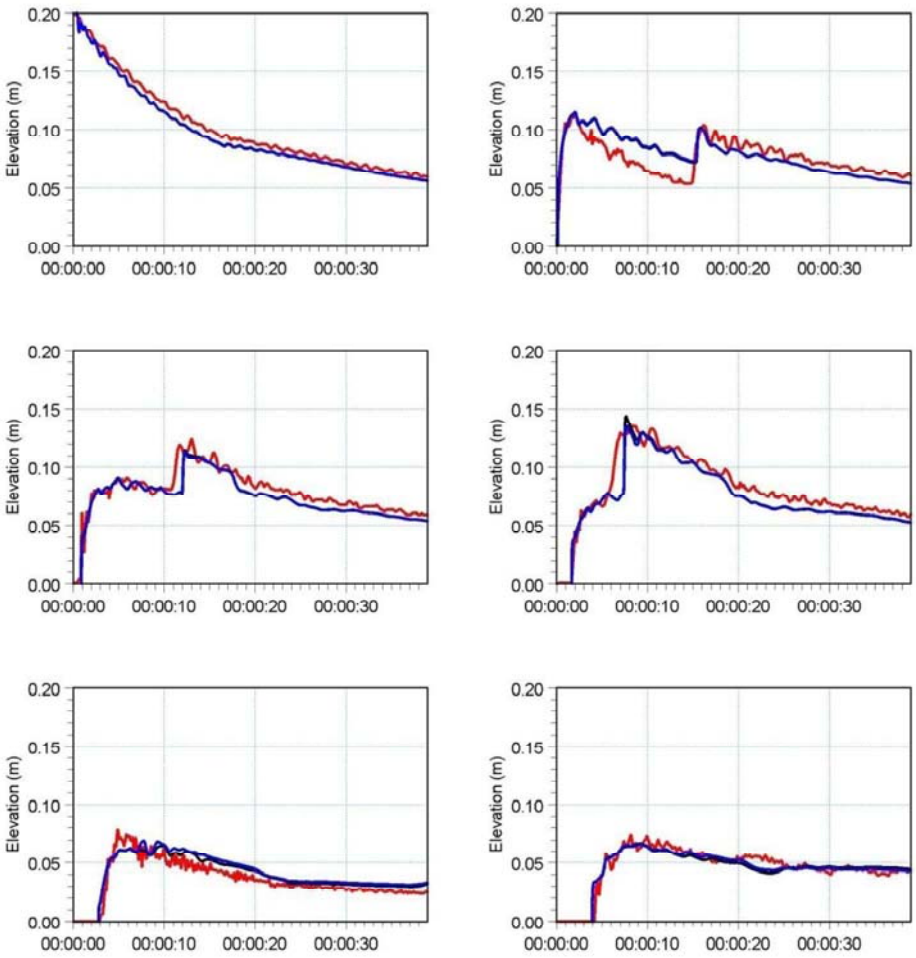

Figure 4.2 Time evolution of the water level at the six gauge locations. (blue) 3D calculation, (black) 2D calculation and (red) Measurements by Frazão and Zech (1999a,b)

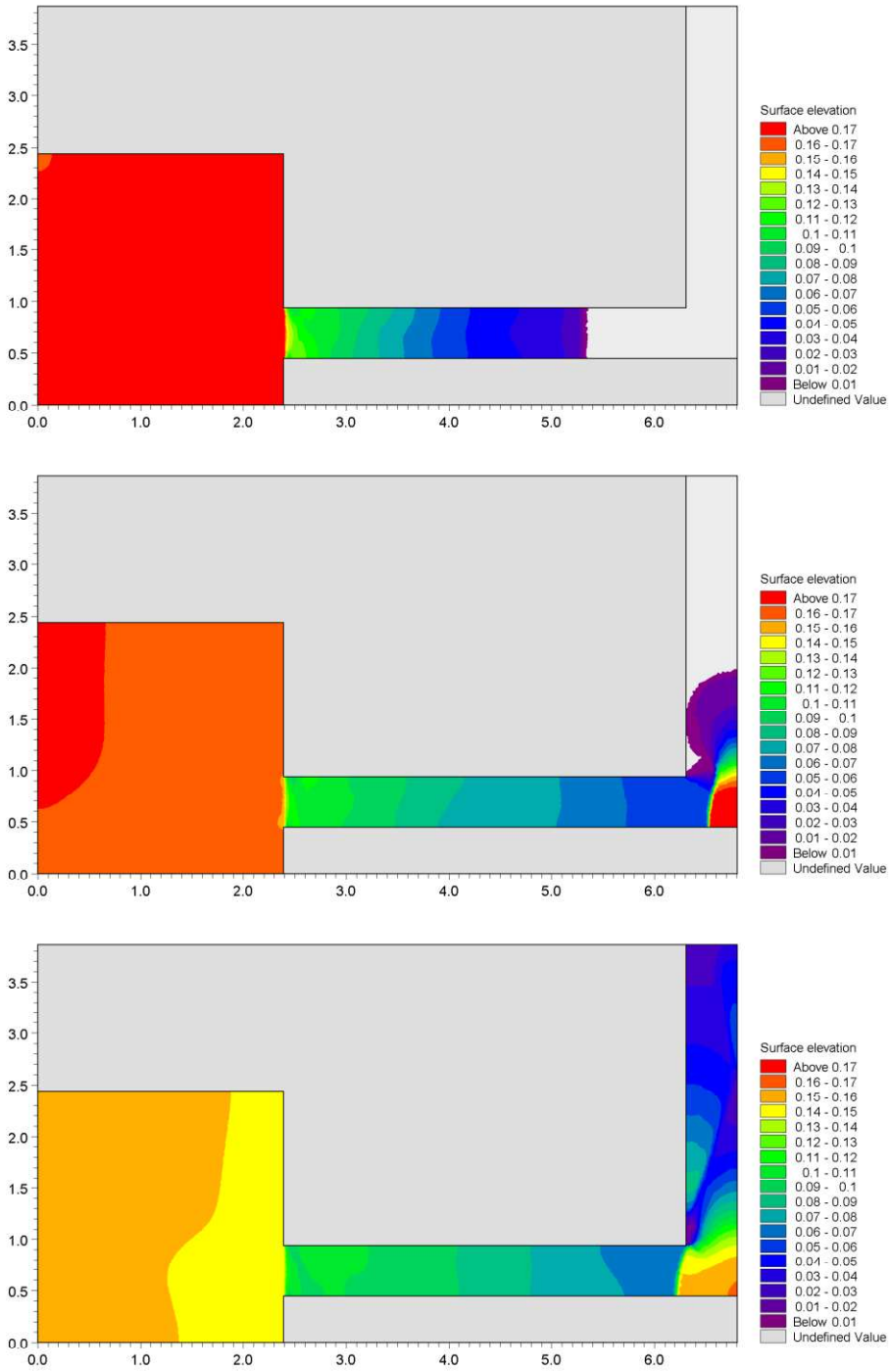

Figure 4.3 Contour plots of the surface elevation at T = 1.6 s (top), T = 3.2 s (middle) and T = 4.8 s (bottom).

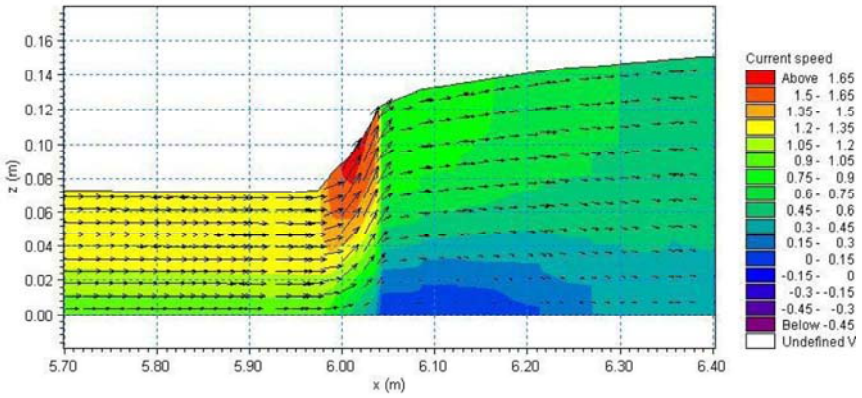

Figure 4.4 Vector plot and contour plots of the current speed at a vertical profile along the centre line at T = 6.4 s

5 REFERENCES

Darwish M.S. and Moukalled F. (2003), *TVD schemes for unstructured grids*, Int. J. of Heat and Mass Transfor, 46, 599-611)

Geernaert G.L. and Plant W.L (1990), *Surface Waves and fluxes, Volume 1 – Current theory*, Kluwer Academic Publishers, The Netherlands.

Hirsch, C. (1990). *Numerical Computation of Internal and External Flows, Volume 2*: Computational Methods for Inviscid and Viscous Flows, Wiley.

Iqbal M. (1983). *An Introduction to solar Radiation,* Academic Press.

Jawahar P. and H. Kamath. (2000). *A high-resolution procedure for Euler and Navier-Stokes computations on unstructured grids*, Journal Comp. Physics, 164, 165-203.

Kantha and Clayson (2000). *Small Scale Processes in Geophysical Fluid flows,* International Geophysics Series, Volume 67.

Munk, W., Anderson, E. (1948), *Notes on the theory of the thermocline,* Journal of Marine Research, 7, 276-295.

Lind & Falkenmark (1972), *Hydrology: en inledning till vattenressursläran,* Studentlitteratur (in Swedish).

Pugh, D.T. (1987), *Tides, surges and mean sea-level: a handbook for engineers and scientists*. Wiley, Chichester, 472pp

Rodi, W. (1984), *Turbulence models and their applications in hydraulics,* IAHR, Delft, the Netherlands.

Rodi, W. (1980), *Turbulence Models and Their Application in Hydraulics - A State of the Art Review,* Special IAHR Publication.

Roe, P. L. (1981), *Approximate Riemann solvers, parameter vectors, and difference-schemes*, Journal of Computational Physics, 43, 357-372.

Sahlberg J. (1984). *A hydrodynamic model for heat contents calculations on lakes at the ice formation date*, Document D4: 1984, Swedish council for Building Research.

Shu C.W. (1997), *Essentially Non-Oscillatory and Weighted Essenetially Non-Oscillatory Schemes for Hyperbolic Conservation Laws*, NASA/CR-97-206253, ICASE Report No. 97-65, NASA Langley Research Center, pp. 83.

Smagorinsky (1963), J. *General Circulation Experiment with the Primitive Equations,* Monthly Weather Review, 91, No. 3, pp 99-164.

Sleigh, P.A., Gaskell, P.H., Bersins, M. and Wright, N.G. (1998*), An unstructured finite-volume algorithm for predicting flow in rivers and estuaries*, Computers & Fluids, Vol. **27**, No. 4, 479-508.

Soares Frazão, S. and Zech, Y. (2002), *Dam-break in channel with 90° bend*, Journal of Hydraulic Engineering, ASCE, 2002, **128**, No. 11, 956-968.

Soares Frazão, S. and Zech, Y. (1999a), *Effects of a sharp bend on dam-break flow*, Proc., 28th IAHR Congress, Graz, Austria, Technical Univ. Graz, Graz, Austria (CD-Rom).

Soares Frazão, S. and Zech, Y. (1999b), *Dam-break flow through sharp bends – Physical model and 2D Boltzmann model validation*, Proc., CADAM Meeting Wallingford, U.K., 2-3 March 1998, European Commission, Brussels, Belgium, 151-169.

UNESCO (1981), *The practical salinity scale 1978 and the international equation of state of seawater 1980*, UNESCO technical papers in marine science, 36, 1981.

Wu, Jin (1994), *The sea surface is aerodynamically rough even under light winds*, Boundary layer Meteorology, 69, 149-158.

Wu, Jin (1980), *Wind-stress Coefficients over sea surface and near neutral conditions – A revisit*, Journal of Physical. Oceanography, 10, 727-740.

Zhao, D.H., Shen, H.W., Tabios, G.Q., Tan, W.Y. and Lai, J.S. (1994), *Finite-volume two-dimensional unsteady-flow model for river basins*, Journal of Hydraulic Engineering, ASCE, 1994, **120**, No. 7, 863-833.

Basic Steps in the MIKE3-FM Temperature Modeling of Don Pedro Reservoir

SET-UP MODEL	✓ Bathymetry and IFSAR Data (3-D surface in GIS) ✓ Model Flexible Mesh and Vertical Layers ✓ Model Boundary Conditions (inflows, air, outflows) ✓ Model Time-step and Simulation Period ✓ Computer Processing Platform
MODEL PARAMETER EVALUATION	✓ Physical Processes Formulated Mathematically ✓ Key Parameters: Heat Exchange & Mixing Coeff's ✓ Initial Evaluation Subject to Adjustment
MODEL CALIBRATION	✓ Comparisons to Field Data (temperature profiles) ✓ Adjust Parameters within Acceptable Ranges
MODEL VERIFICATION	✓ Different Period - No Further Param. Adjustment ✓ Sensitivity Analysis
MODEL PROJECTION BASELINE CONDITIONS	✓ Districts' Current Operations (regs, contractual) ✓ Selection of Hydrological/Meteorological Period ✓ Flows Generated by Water Operations Model

Summary of data needed for Don Pedro Reservoir 3-D temperature model.

Required Data	Source	In Project Database
	Physical and Geomorphological	
Bathymetry	Field survey	yes
Digital Terrain Model (IFSAR)	INTERMAP®	yes
Outlet (invert elevation)	Design drawings	yes
Outlet (lat/long)	Design drawings	yes
Dam spillway (elevation)	Design drawings	yes
Dam spillway (length, type)	Design drawings	yes
Old Don Pedro Dam spillway (elevation)	Design drawings or bathymetric survey	yes
Old Don Pedro Dam spillway (length, type)	Design drawings or bathymetric survey	yes
Old Don Pedro Dam crest (elevation)	Design drawings or bathymetric survey	yes
Old Don Pedro Dam crest (length, type)	Design drawings or bathymetric survey	yes
Old Don Pedro outlet (elevation)	TID	yes
Old Don Pedro outlet (lat/long)	USGS Topographical Map	yes
	Flow and Operations	
Tuolumne River upstream of reservoir (regulated)	CCSF, TID	yes
Tuolumne River upstream of reservoir (total)	TID	yes
Storage (daily)	USGS	yes
Withdrawals through powerhouse (daily)	TID	yes
	Temperature	
Tuolumne River upstream of reservoir	TID (starting October 2010); CCSF, CDFG	yes
Tributaries: Rough & Ready, Moccasin, Sullivan and Woods Creeks	TID (starting April 2011)	yes
Profiles at several locations	CDFG, TID (starting May 2011)	yes
	Meteorology	
Air temperature, wind speed/direction, solar radiation, relative humidity	TID (starting November 2010); WRCC	yes

CCSF City and County of San Francisco
CDFG California Department of Fish and Game
TID Turlock Irrigation District
USGS U.S. Geological Survey
WRCC Western Regional Climate Center

From: Staples, Rose
Sent: Friday, April 06, 2012 6:48 PM
To: 'Alves, Jim'; 'Anderson, Craig'; 'Asay, Lynette'; 'Aud, John'; 'Barnes, James'; 'Barnes, Peter'; 'Blake, Martin'; 'Bond, Jack'; Borovansky, Jenna; 'Boucher, Allison'; 'Bowes, Stephen'; 'Bowman, Art'; 'Brenneman, Beth'; 'Brewer, Doug'; 'Buckley, John'; 'Buckley, Mark'; 'Burt, Charles'; 'Byrd, Tim'; 'Cadagan, Jerry'; 'Carlin, Michael'; 'Charles, Cindy'; 'Cismowski, Gail'; 'Colvin, Tim'; 'Costa, Jan'; 'Cowan, Jeffrey'; 'Cox, Stanley Rob'; 'Cranston, Peggy'; 'Cremeen, Rebecca'; 'Day, Kevin'; 'Day, P'; 'Denean'; 'Derwin, Maryann Moise'; Devine, John; 'Donaldson, Milford Wayne'; 'Dowd, Maggie'; 'Drekmeier, Peter'; 'Edmondson, Steve'; 'Eicher, James'; 'Ferrari, Chandra'; 'Fety, Lauren'; 'Findley, Timothy'; 'Fuller, Reba'; 'Furman, Donn W'; 'Ganteinbein, Julie'; 'Giglio, Deborah'; 'Gorman, Elaine'; 'Grader, Zeke'; 'Gutierrez, Monica'; 'Hackamack, Robert'; 'Hastreiter, James'; 'Hatch, Jenny'; 'Hayat, Zahra'; 'Hayden, Ann'; 'Hellam, Anita'; 'Heyne, Tim'; 'Holley, Thomas'; 'Holm, Lisa'; 'Horn, Jeff'; 'Horn, Timi'; 'Hudelson, Bill'; 'Hughes, Noah'; 'Hughes, Robert'; 'Hume, Noah'; 'Jackman, Jerry'; 'Jackson, Zac'; 'Jennings, William'; 'Jensen, Art'; 'Jensen, Laura'; 'Johannis, Mary'; 'Johnson, Brian'; 'Justin'; 'Keating, Janice'; 'Kempton, Kathryn'; 'Kinney, Teresa'; 'Koepele, Patrick'; 'Kordella, Lesley'; 'Lein, Joseph'; 'Levin, Ellen'; 'Lewis, Reggie'; 'Linkard, David'; 'Looker, Mark'; 'Lwenya, Roselynn'; 'Lyons, Bill'; 'Madden, Dan'; 'Manji, Annie'; 'Marko, Paul'; 'Marshall, Mike'; 'Martin, Michael'; 'Martin, Ramon'; 'Mathiesen, Lloyd'; 'McDaniel, Dan'; 'McDevitt, Ray'; 'McDonnell, Marty'; 'McLain, Jeffrey'; 'Means, Julie'; 'Mills, John'; 'Morningstar Pope, Rhonda'; 'Motola, Mary'; 'O'Brien, Jennifer'; 'Orvis, Tom'; 'Ott, Bob'; 'Ott, Chris'; 'Paul, Duane'; 'Pavich, Steve'; 'Pinhey, Nick'; 'Pool, Richard'; 'Porter, Ruth'; 'Powell, Melissa'; 'Puccini, Stephen'; 'Raeder, Jessie'; 'Ramirez, Tim'; 'Rea, Maria'; 'Reed, Rhonda'; 'Richardson, Kevin'; 'Ridenour, Jim'; 'Robbins, Royal'; 'Romano, David O'; 'Roos-Collins, Richard'; 'Roseman, Jesse'; 'Rothert, Steve'; 'Sandkulla, Nicole'; 'Saunders, Jenan'; 'Schutte, Allison'; 'Sears, William'; 'Shakal, Sarah'; 'Shipley, Robert'; 'Shumway, Vern'; 'Shutes, Chris'; 'Sill, Todd'; 'Slay, Ron'; 'Smith, Jim'; Staples, Rose; 'Steindorf, Dave'; 'Steiner, Dan'; 'Stone, Vicki'; 'Stork, Ron'; 'Stratton, Susan'; 'Taylor, Mary Jane'; 'Terpstra, Thomas'; 'TeVelde, George'; 'Thompson, Larry'; 'Vasquez, Sandy'; 'Verkuil, Colette'; 'Vierra, Chris'; 'Walters, Eric'; 'Wantuck, Richard'; 'Welch, Steve'; 'Wesselman, Eric'; 'Wheeler, Dan'; 'Wheeler, Dave'; 'Wheeler, Douglas'; 'Wilcox, Scott'; 'Williamson, Harry'; 'Willy, Allison'; 'Wilson, Bryan'; 'Winchell, Frank'; 'Wooster, John'; 'Workman, Michelle'; 'Yoshiyama, Ron'; 'Zipser, Wayne'
Subject: LIVE MEETING LINK IF NOT ATTENDING DON PEDRO WORKSHOPS / MEETINGS IN PERSON

If you are unable to attend the upcoming Don Pedro workshops and meetings in person, you will be able to call in (see "AUDIO INFORMATION" below) and you can also use your computer to LIVE MEETING (see individual workshop/meeting links below). If you have not used LIVE MEETING before, please be sure, well before the meeting time, to click on "FIRST ONLINE MEETING" link below. Thank you.

AUDIO INFORMATION
Use call-in number: **866-994-6437**, Conference Code **5424697994**

ON-LINE MEETING INFORMATION
(On-Line Meetings will be open approximately half hour prior to the meeting start time to allow for any technical issues to be resolved. If you have not used On-Line Meeting in the past, please allow a few extra minutes for your first log-on.)

Monday, April 9 (10 am – 5 pm): Hydrology Workshop (W&AR-2)

Join online meeting
https://meet.hdrinc.com/jenna.borovansky/DG5FH7C1

First online meeting?

Tuesday, April 10 (8:30 – 10:15am): Reservoir Temperature Modeling Data and Methods Consultation Meeting (W&AR-3)

Join online meeting
https://meet.hdrinc.com/jenna.borovansky/QC5C5HN1

First online meeting?

Tuesday, April 10 (10:30am – 5:00pm) Salmonid Information Synthesis Workshop (W&AR-5)

Join online meeting
https://meet.hdrinc.com/jenna.borovansky/37NNBCDP

First online meeting?

Wednesday, April 11 (9:00 am – Noon): Temperature Criteria Evaluation Consultation Meeting (W&AR-14)

Join online meeting
https://meet.hdrinc.com/jenna.borovansky/MHVKDJYZ

First online meeting?

ROSE STAPLES
CAP-OM

HDR Engineering, Inc.
Executive Assistant, Hydropower Services

970 Baxter Boulevard, Suite 301 | Portland, ME 04103
207.239.3857 | f: 207.775.1742
rose.staples@hdrinc.com | hdrinc.com

From: Staples, Rose
Sent: Thursday, July 26, 2012 4:39 PM
To: Alves, Jim; Anderson, Craig; Asay, Lynette; Aud, John; Barnes, James; Barnes, Peter; Beniamine Beronia; Blake, Martin; Bond, Jack; Borovansky, Jenna; Boucher, Allison; Bowes, Stephen; Bowman, Art; Brenneman, Beth; Brewer, Doug; Buckley, John; Buckley, Mark; Burt, Charles; Byrd, Tim; Cadagan, Jerry; Carlin, Michael; Charles, Cindy; Colvin, Tim; Costa, Jan; Cowan, Jeffrey; Cox, Stanley Rob; Cranston, Peggy; Cremeen, Rebecca; Damin Nicole; Day, Kevin; Day, P; Denean; Derwin, Maryann Moise; Devine, John; Donaldson, Milford Wayne; Dowd, Maggie; Drekmeier, Peter; Edmondson, Steve; Eicher, James; Fargo, James; Ferranti, Annee; Ferrari, Chandra; Fety, Lauren; Findley, Timothy; Fuller, Reba; Furman, Donn W; Ganteinbein, Julie; Giglio, Deborah; Gorman, Elaine; Grader, Zeke; Gutierrez, Monica; Hackamack, Robert; Hastreiter, James; Hatch, Jenny; Hayat, Zahra; Hayden, Ann; Hellam, Anita; Heyne, Tim; Holley, Thomas; Holm, Lisa; Horn, Jeff; Horn, Timi; Hudelson, Bill; Hughes, Noah; Hughes, Robert; Hume, Noah; Jackman, Jerry; Jackson, Zac; Jennings, William; Jensen, Art; Jensen, Laura; Johannis, Mary; Johnson, Brian; Justin; Keating, Janice; Kempton, Kathryn; Kinney, Teresa; Koepele, Patrick; Kordella, Lesley; Lara, Marco; Lein, Joseph; Levin, Ellen; Lewis, Reggie; Linkard, David; Looker, Mark; Loy, Carin; Lwenya, Roselynn; Lyons, Bill; Madden, Dan; Manji, Annie; Marko, Paul; Marshall, Mike; Martin, Michael; Martin, Ramon; Mathiesen, Lloyd; McDaniel, Dan; McDevitt, Ray; McDonnell, Marty; McLain, Jeffrey; Mein Janis; Mills, John; Minami Amber; Monheit, Susan; Morningstar Pope, Rhonda; Motola, Mary; Murphey, Gretchen; O'Brien, Jennifer; Orvis, Tom; Ott, Bob; Ott, Chris; Paul, Duane; Pavich, Steve; Pinhey, Nick; Pool, Richard; Porter, Ruth; Powell, Melissa; Puccini, Stephen; Raeder, Jessie; Ramirez, Tim; Rea, Maria; Reed, Rhonda; Richardson, Kevin; Ridenour, Jim; Robbins, Royal; Romano, David O; Roos-Collins, Richard; Roseman, Jesse; Rothert, Steve; Sandkulla, Nicole; Saunders, Jenan; Schutte, Allison; Sears, William; Shakal, Sarah; Shipley, Robert; Shumway, Vern; Shutes, Chris; Sill, Todd; Slay, Ron; Smith, Jim; Staples, Rose; Steindorf, Dave; Steiner, Dan; Stone, Vicki; Stork, Ron; Stratton, Susan; Taylor, Mary Jane; Terpstra, Thomas; TeVelde, George; Thompson, Larry; Vasquez, Sandy; Verkuil, Colette; Vierra, Chris; Wantuck, Richard; Welch, Steve; Wesselman, Eric; Wheeler, Dan; Wheeler, Dave; Wheeler, Douglas; Wilcox, Scott; Williamson, Harry; Willy, Allison; Wilson, Bryan; Winchell, Frank; Wooster, John; Workman, Michelle; Yoshiyama, Ron; Zipser, Wayne
Subject: Don Pedro Reservoir Temperature Model April 10 2012 Meeting Notes
Attachments: April 10 2012 Reserv Temp RP Mtg_120726r.pdf

Attached please find Meeting Notes from the Don Pedro Project Relicensing *W&AR-03 Reservoir Temperature Model* meeting held on April 10, 2012.

Action items for the Districts that came out of the meeting are addressed within the notes and model development is proceeding. As requested by the Relicensing Participants, the Districts have postponed the next meeting (originally scheduled for September 18) until mid-October (now scheduled for October 26, 2012) when the Districts will present model verification/calibration, as well as conduct training in use of the model.

NOTE: A copy of this announcement, and the accompanying attachment, are also being uploaded to the INTRODUCTION/ANNOUNCEMENT section of the relicensing website www.donpedro-relicensing.com.

HDR | ONE COMPANY *Many Solutions*℠

Memo

To:	Don Pedro Relicensing Participants		
From:	Turlock Irrigation District / Modesto Irrigation District	Project:	Don Pedro Hydroelectric Project
Date:	July 26, 2012		

Re: Don Pedro Project Reservoir Temperature Model (W&AR-3) Meeting Summary. April 10, 2012

Attendees:

Scott Lowe, HDR
Guy Apicella, HDR
Dale Stanton, CDFG
Bill Johnston, MID
Art Goodwin
Steve Boyd, TID
Bob Nees, TID
Greg Dias, MID
Mike Maher, SWRCB
Tim O'Laughlin (on phone)
Carin Loy, HDR
John Devine, HDR
Jenna Borovansky, HDR
Ronald Yoshiyama, UC Davis
Joy Warren, MID
Annie Manji, CDFG,
Karl English, LGL Limited
Robert Hughes, CDFG

On April 10, 2012, as identified in the FERC-approved study plan, the Districts hosted a meeting at Modesto Irrigation District's offices in Modesto, California, to provide an overview of the MIKE3 model being developed for the Don Pedro Relicensing Study W&AR-3 Reservoir Temperature Modeling Study. Guy Apicella and Scott Lowe of HDR conducted the presentation in which the underlying model physics and assumptions were discussed, as well as the empirical data being used as input, and the nature of the output. Output from the model will consist of simulated temperature responses to changes in hydrological and meteorological drivers as well as simulated project operations.

The modeling task consists of five steps: (1) set up a 3-D flexible mesh; (2) compile input data; (3) calibrate the model; (4) verify the model; and (5) simulate model scenarios. At this time, HDR is setting up the 3-D flexible mesh and compiling all of the input data. Dr. Lowe showed examples of how the mesh looks, discussed some of the choices modelers have when building the mesh, and the two kinds of mesh layering that can be employed to build the vertical dimension of the model—sigma and sigma/z-layer. Using preliminary temperature and bathymetry data, Dr. Lowe also gave an example of how a temperature cross-section might look along an arbitrary line (not the thalweg), pointing out the different temperatures with depth. The differences in interpreting a graphical display of a cross section taken along the thalweg and a cross section taken arbitrarily, like in the example, were pointed out.

Three action items were identified during the meeting:

(1) The Districts will post the PowerPoint presentation from the meeting on the Project web-site. (Posted April 13, 2012, www.donpedro-relicensing.com)
(2) CDFG asked the Districts to provide examples of reservoirs where MIKE3 has been applied by HDR or others (described below).

(3) CDFG asked the Districts to contact DHI and ask if they know of projects where the model's predictions were compared to post-implementation monitoring data (described below).

Examples of MIKE3 Application in Reservoirs

There are numerous examples of other reservoirs, lakes, impoundments, estuaries and bays where MIKE3 has been used for temperature modeling by HDR or others. A brief list of examples of where MIKE3 models have been used by others follows:

- Lake Ontario – various applications by the Ontario Ministry of Environment (OME) and Ontario Power Generation (OPG)
- Lake Simcoe (Ontario, Canada) – by W. F. Baird & Associates
- Lake Michigan – by W. F. Baird & Associates
- Lake Erie - by Great Lakes Unit of Ontario Ministry of Environment
- Hamilton Harbour (off Lake Ontario) – by Cheng He of National Water Research Institute (Canada)
- Lake Esrum (Denmark) – by Rikke Margrethe Closter, Ph.D. thesis at Danish Meteorological Institute
- Fehmarnbelt/Roskilde Fjord (Main entrance to Baltic Sea between Germany and Denmark) – by DHI
- Upper Adriatic Sea and Venice Lagoon (Italy) – by DHI

All the projects are examples of where the MIKE3 model was calibrated by comparing calculated temperature results to measured depth profiles. A description or full report for each of these projects is available by request.

HDR has used MIKE3 models for various projects. Recent applications of the MIKE3-FM model for temperature and/or flow velocities by the team developing the Don Pedro model are:

- Lake Champlain (Vermont and New York)
- Northfield Reservoir (Massachusetts)
- East River (New York) Power Plant Thermal Discharge
- Stalley Bay (St Thomas, USVI)
- Black Dog Cooling Lake (MN)
- Goodman Bay (Bahamas)

The Lake Champlain model was calibrated using measured temperature profiles; the Northfield Reservoir was not calibrated. HDR's report on the Lake Champlain model is posted on www.donpedro-relicensing.com. The Northfield Reservoir model write-up, which covered sediment transport, can also be found at www.donpedro-relicensing.com.

In addition to the temperature applications above, the HDR team has also applied MIKE3 to these waterways for non-temperature (e.g., water quality, sediment) modeling:

- Lake Jessup (FL)
- Jamaica Bay (NY)

- New York Harbor (NY)
- Long Island Sound (NY-CT-RI)
- Hudson River (NY)
- Newark Bay (NJ)

Model Predictions versus Actual

CDFG also asked if the MIKE3 model temperature projections were ever compared to temperature monitoring data collected in the future (versus historical data). HDR could not find information that documented such a comparison and, when contacted, DHI was not able to provide examples.

Path Forward

HDR indicated that model development was proceeding. The Districts will provide an update in the summer and then hold a meeting in mid-October to present model verification/calibration and conduct training in use of the model.